



Physical properties of the organic aerosols and clouds on Titan

C.P. McKay^{a,*}, A. Coustenis^b, R.E. Samuelson^c, M.T. Lemmon^d, R.D. Lorenz^d, M. Cabane^e,
P. Rannou^e, P. Drossart^f

^aNASA Ames Research Center, Moffett Field, CA 94035, USA

^bDESPA, Observatoire de Paris-Meudon, 92195 Meudon, France

^cNASA/GSFC, Greenbelt, MD 20771, USA

^dL.P.L., Univ. of Arizona, Tucson, AZ 85721, USA

^eService d'Aéronomie, Univ. de Paris 6, 75252 Paris France

^fDESPA, Observatoire de Paris-Meudon, 92195 Meudon, France

Received 18 October 1999; received in revised form 19 April 2000; accepted 26 April 2000

Abstract

Titan's haze is optically thick in the visible, with an optical depth at 0.5 μm of about three. The haze varies with latitude in a seasonal cycle and has a detached upper layer. Microphysical models, photochemical models, and laboratory simulations all imply that the production rate of the haze is in the range of $0.5\text{--}2 \times 10^{-14} \text{ g cm}^{-2} \text{ s}^{-1}$. Given the rate of sedimentation, the total mass loading is about 250 mg m^{-2} . The transparency of the haze is high for wavelengths above $1 \mu\text{m}$ because the haze material becomes almost purely scattering and the optical depth decreases with increasing wavelength. The particles in the main haze deck are probably fractal in structure with an equivalent volume radius of $0.2 \mu\text{m}$. The haze material is organic and, if similar to laboratory tholin, has a C/N ratio in the range of 2–4 and a C/H ratio of about unity. The haze significantly affects the thermal balance of Titan, causing an anti-greenhouse effect that cools the surface by 9 K. Titan's faintly banded appearance suggests strong zonal winds in the lower stratosphere. Condensate clouds of ethane or methane, if present, are thin, patchy, or transient. Stratospheric clouds of condensed nitriles and (possibly) hydrocarbons appear to be associated with, though not contained entirely in, the polar shadow, suggesting abundances may vary with the season. Precipitating condensate particles from the stratosphere probably act as nucleating centers for the formation and rapid growth of methane ice particles in the troposphere, where the gas phase appears to be highly supersaturated. Once formed, fallout times for these hailstones are $\sim 2 \text{ h}$ or less. Melting, and possible subsequent fragmentation of methane raindrops should occur at $\sim 12 \text{ km}$ and below. Almost complete evaporation should occur just above the surface. A thin residue of ethane-enriched fog particles would then slowly settle to the surface, steadily modifying an existing surface or subsurface residue of liquid hydrocarbons. The optical properties of the haze in the 1 to 3 μm spectral region and the implications for the visibility of the surface are probably the most pressing current research questions. Other key questions include the nature of the high altitude detached haze layer, altitude and seasonal changes in composition of the haze, the role of haze particles as condensation nuclei for clouds, and the nature of any condensate clouds. Published by Elsevier Science Ltd.

1. Introduction

The surface pressure of Titan is 50% greater than that of the Earth. The temperature at the surface is close to 94 K, decreasing to about 71 K at the tropopause, which is located at an altitude of 40 km (Samuelson et al., 1981; Lindal et al., 1983; Lellouch et al., 1989). Above the tropopause, the temperature rises rapidly to 160–180 K (Lellouch et al., 1989). The atmosphere is composed pri-

marily of N_2 with less than 8% CH_4 . These molecules are the parent species for an active photochemistry resulting in the production of many hydrocarbons and nitriles in the stratosphere (Yung et al., 1984). Further chemistry and phase changes in the thermal environment of the stratosphere lead to the production of an extensive system of organic clouds and aerosols.

Our understanding of Titan's atmosphere has evolved over several decades (for a previous review see Hunten et al., 1984). Early Earth-based observations revealed the presence of an atmosphere containing substantial amounts of CH_4 (Kuiper, 1944; Trafton, 1972). Polarization

* Corresponding author. Fax: +001-415-604-6779.

E-mail address: cmckay@arc.nasa.gov (C.P. McKay).

observations by Veverka (1973) and Zellner (1973) indicated the presence of an important solid-phase component. The presence of CH₄ and the reddish color of this hazy material led to the suggestion that solid organic aerosols were being produced in Titan's atmosphere by CH₄ photolysis (Khare and Sagan, 1973). Danielson et al. (1973) suggested that absorption of solar radiation by this haze led to a strong thermal inversion in Titan's atmosphere, accounting for the unexpectedly high infrared brightness temperatures observed between 8 and 14 μm by Low (1965), Allen and Murdock (1971), and Gillett et al. (1973).

This basic picture of the organic nature of Titan's atmosphere (reviewed by Chang et al., 1979) was confirmed by the Voyager observations of Titan in 1980. Voyager images showed an optically thick haze in the stratosphere completely obscuring the surface at visible wavelengths (Smith et al., 1981, 1982; Rages et al., 1983). The presence of CH₄ and direct detection of other organic compounds by Voyager (Hanel et al., 1981; Maguire et al., 1981; Kunde et al., 1981) supported the conjecture that this haze is composed of photochemically produced solid organic matter (Khare et al., 1984; Sagan and Thompson, 1984). The haze has a dominant influence on the propagation of solar radiation in Titan's atmosphere and thereby has a significant effect on the temperature structure of the atmosphere and the surface temperature (Danielson et al., 1973; Samuelson, 1983; McKay et al., 1989, 1991).

Laboratory simulations have been carried out in an effort to reproduce the solid organic material thought to compose the Titan haze. The optical properties of the laboratory material – tholin – match the broad features of the geometric albedo spectrum of Titan (Khare et al., 1984) and can fit detailed microphysical and radiative simulations with both spherical particles (McKay et al., 1989; Toon et al., 1992) and fractal particles (Rannou et al., 1995; Tomasko et al., 1997) – with a better fit obtained with the fractal particles. If tholin provides a good analogue for the Titan haze then we can conclude that the haze is composed of refractory organics that, once condensed, do not evaporate and are ultimately deposited on Titan's surface.

Much of the information on clouds and condensates in Titan's atmosphere is indirect. Nominal temperature profiles (e.g. Lellouch et al., 1989) for the lower atmosphere of Titan inferred from Voyager 1 data suggested that the CH₄ abundance there is high enough that concentrations will reach saturation in the upper troposphere. Thus CH₄ clouds might be expected to form. Initially, two indirect pieces of evidence suggested the possibility of such clouds: increased scintillation in the Voyager 1 radio occultation data at the level where CH₄ cloud formation was expected (Hinson and Tyler, 1983), and the need for an additional opacity source in the upper troposphere in order to explain the observed infrared continuum between 200 and 600 cm^{-1} (Samuelson et al., 1981). The latter suggestion was based on the collision-induced absorption coef-

ficients that were available at the time, especially those involving methane.

On the other hand, theoretical considerations suggested that conditions in Titan's troposphere were likely to be incompatible with extensive CH₄ cloud cover. Toon et al. (1988) suggested that, because of the relative scarcity of seed nuclei, CH₄ droplets would rapidly grow to large sizes, $\sim 100 \mu\text{m}$. Since such large particles would quickly precipitate they should be optically thin, forming rain without clouds. Based on analysis of the thermal balance McKay et al. (1989) concluded that clouds, if present, were patchy or thin. Finally, Courtin et al. (1995) and Samuelson et al. (1997b), based on new collision induced absorption coefficients that had recently become available (especially those for N₂–CH₄; see, e.g. Borysow and Tang, 1993), suggested that large CH₄ supersaturation might be required to account for the intensity of the spectral continuum between 200 and 600 cm^{-1} . This would be consistent with the absence of clouds or with cloud particle growth limited by the availability of condensation nuclei (Samuelson and Mayo, 1997; Guez et al., 1997). McKay et al. (1997) suggested that the absence of moist convection in Titan's troposphere is consistent with a lack of clouds. Griffith et al. (1991), based on observations in the near infrared (2 μm), also concluded that tropospheric clouds were patchy or thin. Imaging of the surface of Titan in the near infrared by HST (Smith et al., 1996) has not provided evidence for clouds. Recently, Griffith et al. (1998) have reported an anomalous feature in the IR spectrum for two nights consistent with methane clouds at 15 km covering 9% of the disk.

In addition to possible CH₄ clouds in the troposphere, condensate layers may exist in the stratosphere. Almost all primary by-products of the stratospheric photochemistry are sufficiently abundant to condense in the cold, lower reaches of the stratosphere, with the exceptions of CO, H₂, and possibly C₂H₄ (Maguire et al., 1981; Sagan and Thompson, 1984). Thus, many ice clouds of differing composition may occupy much of this region, provided viable seed nuclei are present to promote condensation. As with CH₄ clouds, there is not yet direct detection of these condensate layers at low latitudes and there is the possibility that they do not form due to inhibition of condensation, as suggested for Neptune (Moses et al., 1992) and inferred from the insolubility of laboratory tholin in liquid ethane (McKay, 1996). However, it is not clear that solubility can be directly correlated with condensation efficiency, particularly for the solid phase (e.g. Pruppacher and Klett, 1978). Furthermore, Voyager 1 infrared spectra taken near the north polar hood at grazing incidence show broad features not attributable to gases. The 478 cm^{-1} feature was identified as the ν_8 band of C₄N₂ ice by Khanna et al. (1987), and quantitatively analyzed by Samuelson et al. (1997a).

Considerable effort has been directed toward observations and models investigating the nature of the organic

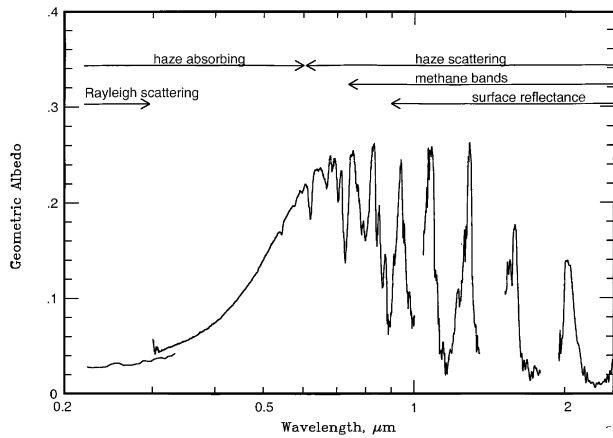


Fig. 1. The geometric albedo of Titan: from IUE data (McGrath et al. 1998), 0.2–0.3 μm ; from Karkoschka (1990), 0.3–1 μm ; for wavelengths beyond 1 μm see Coustenis et al. (1998a) for the leading side of Titan. Also shown in this figure are the processes which contribute to the albedo in each wavelength range.

haze in Titan's atmosphere. Laboratory simulations have played a key role in elucidating the chemical nature of the haze material and have provided useful constraints on the elemental composition, solubility, and optical properties of the organic matter in the haze. Computer simulations of haze formation have provided information on the rate of haze production and the physical properties of the haze particles. In the following sections we review in detail our present understanding of the haze and clouds in Titan's atmosphere, emphasizing physical processes inferred or derived from the wealth of observational data available. We also consider key questions that might be resolved with upcoming remote sensing observations of the Cassini orbiter, or with data from the Huygens probe.

2. Relevant observations

2.1. UV, visible, and near-IR spectroscopy

The geometric albedo of Titan as a function of wavelength was the first, and remains the most useful data set, for understanding the nature of the haze. Fig. 1 shows a recent data set as compiled by Karkoschka (1994, 1998) from 0.3–1 μm , together with the IUE data from McGrath et al. (1998) from 0.2–0.3 μm and data for wavelengths beyond 1 μm from Coustenis et al. (1995). Also shown in this figure are the processes which determine the albedo in each wavelength range.

In the UV, the geometric albedo is determined by the relative opacity of the dark absorbing haze material and the bright Rayleigh scattering of the gas (Courtin et al., 1991). In the visible, the albedo is determined entirely by the properties of the haze, which is optically thick at

these wavelengths. Gas opacities are negligible and the haze completely obscures the surface. This spectral region is useful for determining the production rate of the haze material as well as its optical properties in the upper atmosphere (McKay et al., 1989). At longer wavelengths, $>0.6 \mu\text{m}$, the scattering extinction efficiency of the particles decreases due to the increasing ratio of wavelength to particle size. More importantly, the haze material – based on the tholin analogue (Khare et al., 1984) – becomes virtually non-absorbing. Thus, at wavelengths beyond 0.6 μm , the haze becomes progressively more transparent and the surface properties influence the observed albedo (Fig. 6 of McKay et al., 1989). However, near 0.8 μm CH_4 absorption features become prominent. Thus in this spectral region the albedo is determined by the CH_4 amount, the surface properties, and, to a lesser extent, by the haze (McKay et al., 1989; Coustenis et al., 1995), although the shapes of the band wings are affected by the relative abundances of haze and CH_4 .

Ground-based spectroscopic observations in the near-IR methane windows between 0.9 and 2.5 μm by Griffith (1993), Lemmon et al. (1993, 1995) and Coustenis et al. (1995, 2000b) show a time variability of albedo commensurate with orbital phase around Saturn. This implies that Titan is phase-locked with Saturn, and that the haze is sufficiently translucent in the windows to reveal a noticeable longitudinal variation in surface albedo. The geometric albedo of Titan has also undergone small oscillations over the past two decades, with variations of $10 \pm 1.3\%$ at 0.47 μm and $7 \pm 1.3\%$ at 0.55 μm that correlate with the seasonal cycle (Lockwood, 1977; Lockwood and Thompson, 1979; Lockwood et al., 1986). These variations appear to be atmospheric in origin, and suggest that Titan's haze varies regularly with season.

Some evidence is available for the occasional existence of tropospheric clouds. Spectra of Titan taken by Griffith et al. (1998) with the CGS4 spectrometer of the United Kingdom Infrared Telescope (UKIRT) on September 4 and 5, 1995, show unexpected albedo enhancements compared with 16 other UKIRT spectra. In particular, albedos derived from the September 5 data exceed those previously measured at the same Titan longitude by 14, 17, 30, and 200% in the 1.3, 1.6, 2.0, and 2.9 μm methane windows, respectively. Deviations of the September 5 spectrum from other (nominal) spectra begin at a wavelength of $\approx 2.15 \mu\text{m}$, where the atmospheric weighting function is relatively narrow and peaks at $\sim 15 \text{ km}$. Regions of the spectrum at slightly shorter wavelengths are associated with greater atmospheric transparency and show enhanced albedos, whereas spectral regions at slightly longer wavelengths are associated with lesser transparency and show albedos almost identical with nominal (unenhanced) spectra. This strongly suggests an effective reflecting level at an altitude of $\sim 15 \text{ km}$ in the September 5 data, consistent with a tropospheric methane cloud at that level covering about 9% of Titan's disk.

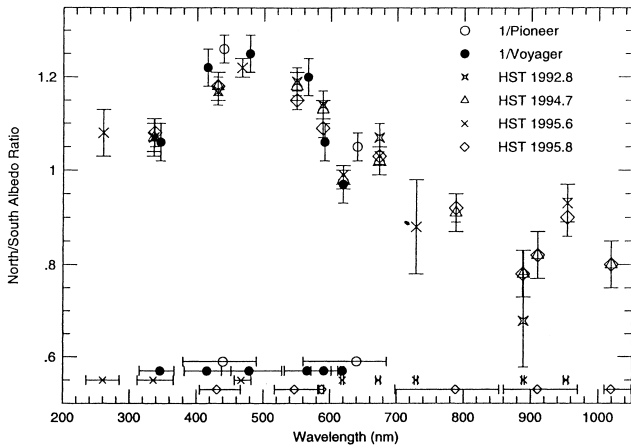


Fig. 2. Wavelength dependence of the North/South albedo ratio from HST measurements. To account for a phase lag of about one half of the seasonal cycle, the reciprocals of the Voyager and Pioneer data are actually plotted. Horizontal bars at the bottom indicate the wavelength coverage of the filters used (from Lorenz et al., 1997).

2.2. Imaging and photopolarimetry

Voyager imaging of Titan in the visible range revealed a marked hemispherical asymmetry in the brightness of the haze (Sromovsky et al., 1981). Specifically, at the season when Voyager observed Titan (northern spring), the southern hemisphere had an albedo about 25% brighter than the north at blue wavelengths, with the interhemispheric contrast smaller at green and violet wavelengths. Lorenz et al. (1997) investigated these and other Voyager images and found that the UV and orange albedo asymmetries are less extreme even than the green and violet values. These authors also examined a number of HST images at visible, UV and near-IR wavelengths, and determined limb-darkening coefficients as a function of wavelength for both these and certain Voyager images. The north/south albedo ratios are shown in Fig. 2 and provide information on the spectral characteristics of the haze. Lorenz et al. (1997) suggest that a change in particle number density between 70 and 120 km could explain the observed asymmetry. Recently Lorenz et al. (1999) used WFPC-2 observations of Titan over several years to show that the phasing of the variations in interhemispheric contrast is wavelength dependent with contrast changes in the blue lagging behind changes in the violet and yellow/red.

In Voyager observations of the brightness at high phase angles (Rages and Pollack, 1983), particles are observed at altitudes as high as 500 km above the surface. A planet-wide detached haze layer occurs between 300 and 350 km above the surface; the visible limb of the planet, where the vertical haze optical depth is 0.1, is about 220 km above the surface. Fig. 3 shows a typical profile of the vertical extinction due to the haze layer. The upper detached haze layer is clearly evident.

Spacecraft data have also provided information on the scattering properties of the haze particles. Data from Pioneer 11 and Voyager photopolarimetry (Tomasko and Smith, 1982; West et al., 1983) showed large positive polarization at $\sim 90^\circ$ phase angle. This requires particles, if spherical in shape, with radii no larger than 0.1 μm . However, Voyager observations (Rages et al., 1983) of the brightness of Titan at high phase angles require particles that are at least 0.2 μm and probably 0.5 μm in radius. Thus, Titan's haze cannot consist of simple spherical particles, and it is now believed that they are non-spherical aggregates of small, roughly spherical monomers (West and Smith, 1991; Rannou et al., 1995; Karkoschka and Lorenz, 1997; Tomasko et al., 1997).

Caldwell et al. (1992), using the original Hubble Space Telescope (HST) WFPC camera, compared images of Titan with those obtained 9 and 10 yr earlier by Voyager. At blue and green wavelengths the north–south asymmetry appeared to have reversed, which is attributed to seasonal change. They also noted that the asymmetry seen in a methane band image at 889 nm appeared to have a structure opposite from that seen at visible wavelengths.

Smith et al. (1996) report observations using WFPC-2 at near-IR wavelengths covering methane windows at 0.94 and 1.07 μm . These images also show a strong north–south asymmetry, as well as limb brightening. After these effects have been removed, however, it is possible to discriminate surface features, at contrasts of about 5–10% of the total brightness. The ability to image the surface implies that the haze and any clouds are transmitting light at these wavelengths due to scattering, but not necessarily that they are optically thin. Smith et al. (1996) also analyzed an image of Titan at 673 nm, which does not show the same marked north–south asymmetry, or limb brightening. Surface features could also be detected, although at very poor contrast, due to the increased optical depth and absorption at these wavelengths.

Spatially resolved images of Titan from ground-based telescopes have been acquired in recent years by several groups. Images were acquired at 1.3, 1.6 and 2.0 μm using the adaptive optics system ADONIS at the ESO telescope in Chile (Combes et al., 1997), and at 1.3, and 1.6 μm in 1997 and 1998, using the adaptive optics system PUEO at the Canadian French Hawaiian (CFHT) telescope in Hawaii (Coustenis et al., 2000a). Gibbard et al. (1999) used speckle imaging on the Keck I telescope to image Titan at 1.6 and 2.1 μm . These images confirm the bright area (distinguished as 2 or possibly 3 independent regions) near the equator on the bright hemisphere of Titan (Combes et al., 1997; Gibbard et al., 1999). Images taken with narrow filters near 2.1 μm (in the methane band) show a sharp north–south asymmetry in the stratosphere of Titan, and a bright south limb, consistent with the expected aerosol concentration in the south pole at this epoch, reversed with respect to the Voyager encounters. Further analyses of the 1.0–2.0 μm images (within the methane windows) (Combes et al., 1997; Gibbard

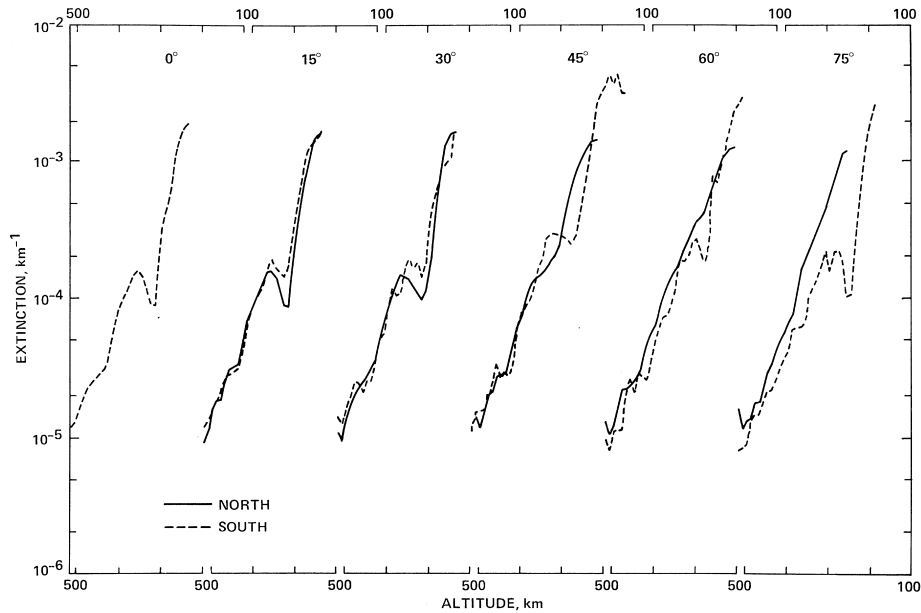


Fig. 3. Extinction profiles of the haze from Rages and Pollack (1983), showing the upper detached layer from 300 to 350 km and the enhancement of extinction near the north pole at the time of Voyager observations, November 1980.

et al., 1999), combined with modeling of recent spectroscopic data, indicate that there are other bright regions present on the surface of Titan at high latitudes. Overall the IR observations suggest that the surface of Titan is visible through the haze in the near infrared.

Gibbard et al. (1999) reported the existence of dark regions (albedo < 0.05), possibly hydrocarbon lakes. In addition to obtaining an albedo map of the surface Gibbard et al. (1999) determined the opacity of the atmosphere to be 0.14 and 0.45 at $1.6 \mu\text{m}$ in the northern and southern hemisphere, respectively. The corresponding values at $2.1 \mu\text{m}$ are 0.30 and 0.1.

Despite the work listed above the question of the optical properties of the haze in the methane windows from 1 to $3 \mu\text{m}$ and the related question of the surface albedo at these wavelengths remain uncertain. Current observations and models are not precise enough to specify these parameters at levels that can be used for planning Cassini imaging of Titan.

Karkoschka and Lorenz (1997) analyzed HST images of Titan and Saturn taken near the August 1995 ring-plane crossing. These images show Titan's shadow cast onto Saturn, as well as Saturn's rings edge-on. The shadow measurements are analogous to those made in the high-phase angle Voyager image analysis by Rages and Pollack (1983), although the rings could act as a fiducial marker to determine the location of Titan's center in the HST data; no such marker was available in the Voyager data.

Using the shadow data, Karkoschka and Lorenz (1997) were able to show that the altitude of the optical limb is between 10 and 128 km lower (depending on wavelength)

in a region southward of 45°S , compared with north of the equator. Assuming an aerosol profile with spherical particles, they determined that the aerosols in the northern region are around $0.3 \mu\text{m}$ in radius, while those in the south are smaller, around $0.1 \mu\text{m}$ in radius. This model fails slightly in the UV, where the data indicate a slightly higher limb than the models suggest – they attribute this to the non-spherical (probably fractal) nature of the aerosol particles. The northern $0.3 \mu\text{m}$ and the smaller southern particles possibly reflect the populations of two separate aerosol layers – with the upper “detached” layer only present in the north.

2.3. Stellar occultation measurements

Knowledge of Titan's atmosphere was usefully augmented by observations of the occultation of the relatively bright star 28 Sgr by Titan in July 1989. The data allowed an estimation of the scale height and temperature at an altitude of about 450 km (a region not well investigated by Voyager instrumentation) and suggested that Titan's atmosphere is not spherically symmetric (Hubbard et al., 1993). Sicardy et al. (1990) estimated an oblateness of 0.017 at an altitude of 250 km (0.25 mbar). Further analysis of the data (Hubbard et al., 1993) established that a simple oblateness does not adequately reproduce the data. Detailed inversion of the occultation lightcurves yields a shape consistent with the zonal wind profile suggested by GCM simulations (Hourdin et al., 1995). Further, the occultation measurements are able to constrain the optical depth of the haze. Specifically, at a reference altitude of 318 km and a reference wavelength of $0.5 \mu\text{m}$, Hubbard et al. derive tangential optical path lengths

of 0.084–0.183 for the low haze layer and of 0.628–3.35 for the high haze layer, and scale heights of 12.7–18 km for the low and 9.7–18 km for the high haze layer.

The low haze is present globally. The higher haze layer is present in their model only northward of about 20°S. This is the opposite of the asymmetry noted by Toon et al. (1992) from Voyager and Pioneer data, where the high “detached” haze layer is present in the southern hemisphere and at low and mid-northern latitudes. Hubbard et al. (1993) find their haze scale heights are smaller than the values deduced by Rages and Pollack (1983), and their occultation-derived haze is higher in altitude by one pressure scale height. It is emphasized that no discrepancy is necessarily implied by this disagreement – the 28 Sgr occultation occurred at virtually northern midsummer, while the Voyager encounters occurred about 8 yr earlier, in Titan’s northern spring. Clearly a seasonal dependence could account for the difference.

Hubbard et al. (1993) also suggest that there may be a slight systematic enhancement of the haze opacity on the sunrise side of Titan. Further, it may be necessary to invoke regional variations in haze opacity on small scales to fit their entire data set.

2.4. Far-IR spectroscopy

A special Voyager 1 limb-tangent viewing sequence with the IRIS instrument enabled Samuelson and Mayo (1991) to infer far infrared properties of the aerosol in the north polar region of Titan’s lower stratosphere. They found that the stratospheric continuum opacity increased monotonically between 250 and 600 cm⁻¹, and that this increase becomes exacerbated with decreasing altitude. These properties would be compatible with an aerosol consisting of very small particles at higher altitudes, with an additional large-particle component lower down, but still above the tropopause. Originally Samuelson and Mayo thought that this wavenumber-dependence of opacity precluded hydrocarbon condensates from being responsible for the large-particle component. However, once it was realized that scattering, rather than absorption, was probably the dominant extinction mechanism, ethane condensate clouds consisting of particles with radii $r \leq 10 \mu\text{m}$ became a viable candidate (Samuelson and Mayo, 1997). Maximum normal optical thicknesses for the entire stratosphere are on the order of ~ 0.15 at 600 cm⁻¹ and about an order of magnitude less at 250 cm⁻¹. Most of this opacity is due to the large-particle component in the lower part of the stratosphere. An aerosol mass mixing ratio of $\sim 6 \times 10^{-8}$ is inferred at an altitude of 160 km. Samuelson and Mayo (1991) also inferred that the scale height of the aerosol is about 1.5 times the atmospheric density scale height, although the large particle component lower down has a smaller scale height. Uncertainties in vertical temperature gradient could cause systematic errors in these values.

Far infrared opacities of the haze are less certain at other latitudes on Titan. Samuelson et al. (1997b) inferred the wavenumber dependence of the aerosol at the latitude of the ingress radio occultation point ($\sim 6^\circ \text{N}$). Once again the opacity appears to increase monotonically from 250 to 600 cm⁻¹, and in fact is very similar to that of the tholin residue found in the laboratory by Khare et al. (1984). Assuming the same wavenumber dependence for the high-latitude aerosol, Samuelson et al. inferred that, within the uncertainties of the data, the stratospheric aerosol opacity is roughly independent of latitude, except for an apparent reduction of opacity at high southern latitudes to about 70% of that elsewhere.

Qualitatively this is similar to the latitudinal dependence of haze opacity found by Rages and Pollack (1983) at altitudes of ~ 250 km, based on Voyager 2 images of Titan’s limb. Quantitatively the drop in opacity at high southern latitudes is more severe at visual wavelengths, being reduced to less than 50% of what it is at other latitudes.

This general trend is somewhat similar to results obtained by Coustenis and Bézard (1995), based on IRIS data at 650, 900, 1000, and 1100 cm⁻¹. However, this latter analysis also shows an increase in stratospheric opacity by a factor 2 or more at latitudes above 50° N with respect to mid- or southern latitudes. The far-IR spectra are more sensitive to conditions in the lower stratosphere than are the imaging data, and any enhancement of opacities in the north polar hood due to condensates might be expected to be manifested more readily at thermal wavelengths. The higher IR wavenumbers examined by Coustenis and Bézard are sensitive to smaller numbers of large particles than are the lower wavenumbers considered by Samuelson et al. and are also less affected by emission from the troposphere.

However, all analyses of thermal measurements are extremely sensitive to the temperature profile adopted, and no direct determinations of temperatures in the lower stratosphere, where condensates are expected, were possible. As a result, uncertainties in thermal opacities at these altitudes are large and may partially account for the somewhat disparate results of Coustenis and Bézard on the one hand, and Samuelson et al. on the other. The CIRS infrared spectrometer on board Cassini will have the capability of inferring temperatures independently at these altitudes from data around 70 cm⁻¹, where N₂–N₂ collision induced opacity is important.

3. Laboratory simulations of Titan’s haze

Since the early work of Khare and Sagan (1973) many laboratory simulations of Titan’s atmosphere have been conducted. In these simulations, gas mixtures with the composition of Titan’s atmosphere that are irradiated with UV light, electrical discharge, or energetic electrons have

Table 1
Comparison of elemental composition of tholin

Reference	Stoichiometry	C/N ratio	Conditions
Sagan et al. (1984)	C ₈ H ₁₃ N ₄	1.9	Low P
Coll et al. (1995)	C ₁₁ H ₁₁ N	11	Low T
McKay (1996)	C ₁₁ H ₁₁ N ₂	5.5	High T,P
Coll et al. (1999)	C ₁₁ H ₄ N ₁₄	2.8	Low T,P

produced a solid organic material – termed tholin – which has optical properties similar to those needed to match the geometric albedo of Titan (Rages and Pollack, 1980; McKay et al., 1989). Khare et al. (1984) determined the real and imaginary indices of refraction for a tholin produced from the passage of a DC electrical discharge through a mixture of 10% CH₄–90% N₂ at standard temperature and a pressure of 0.2 mbar.

Considerable work has been directed toward investigating organic syntheses from mixtures that represent the products of N₂–CH₄ photochemistry such as C₂H₂ and HCN. Using electron microscopy observations of photochemically produced particles in Ar–C₂H₂ mixtures, Bar-Nun et al. (1988) observed that either spherical particles or aggregates built from spherical monomers can be formed, implying that the growing aerosols do not behave as liquid drops and that they can stick together to form clusters. Such particles were also observed by Scattergood et al. (1992) in C₂H₂ mixtures with He or N₂. Clarke and Ferris (1997) studied the formation of particles from HC₃N and C₂H₂. In general these studies may be illustrative but they do not correspond to the mixture of gases on Titan.

Coll et al. (1995, 1998) have conducted Titan simulations with CH₄ and N₂ at temperatures and pressures of Titan's stratosphere and have analyzed the products without exposing them to air. These results promise to give the most accurate simulation of Titan's haze formation to date. Future simulations and models may want to incorporate trace amounts of oxygen to account for the H₂O, CO, and CO₂ abundances on Titan, discovered respectively by Coustenis et al. (1998), Lutz et al. (1983), and Samuelson et al. (1983).

Several groups have used the laboratory simulations to determine the molecular and elemental composition of the Titan haze. Detailed analysis of the organic compounds contained in tholin (Raulin, 1985; Khare et al., 1987; Thompson et al., 1991) show that they include a complex organic mix of simple alkanes, aromatic compounds, heteropolymers, and amino acid precursors.

In addition to the organic structure, there is interest in the simple elemental composition of the haze in order to determine its importance as a sink for photochemical products. It also provides a simple diagnostic parameter for bulk comparison of tholins produced under different conditions. Table 1 compares the elemental composition of the haze as determined by laboratory simulations. As is

evident from this table the results vary widely, probably owing to changes in the temperature and pressure of the simulations and the energy source used. Because of the importance of temperature in the condensation process it is likely that the low temperature results of Coll et al. (1999) represent the most accurate simulation. Laboratory simulations at higher temperatures apparently underestimate the incorporation of carbon-containing compounds into the haze material by up to a factor of 2.

McKay (1996) considered the photolysis rate of CH₄, the dissociation rate of N₂, and the production rate of tholin, and derived column number densities for both carbon and nitrogen atoms, as well as the total column mass (Table 2). The CH₄ and N₂ dissociation rates are from Toublanc et al. (1995); the haze production rate is from McKay et al. (1989) and is typical of the values in Table 3. The elemental composition of the haze material is based upon laboratory tholin results summarized in Table 1, using an average value of the C/N ratio of 4. McKay (1996) concluded that the production of tholin on Titan is a minor sink for C but not for N. About 12% of the N produced is lost as solid organic material. This sink of N atoms is large enough that it must be accounted for in a self-consistent way in photochemical models of Titan's atmosphere. This is particularly important if, as is likely, the N incorporated into the haze derives from HCN. The rate of HCN production in current photochemical models (e.g. Toublanc et al., 1995) is comparable to the sink of N in haze material listed in Table 2. It is likely that the computed profiles of HCN will be altered when this additional sink of N is included. This could be important because the HCN profile determined by Tanguy et al. (1990) is currently being used to infer the eddy diffusion coefficient (Toon et al., 1992; Toublanc et al., 1995). Indeed, Lara et al. (1996) have found that the eddy diffusion coefficient derived from the HCN values is too large to be consistent with the distribution of hydrocarbons. Including an important additional sink for HCN could resolve this discrepancy as shown by Lara et al. (1999).

Regarding the loss of carbon in haze material, current photochemical models (Yung et al., 1984; Toublanc et al., 1995; Lara et al., 1996) already include the loss of C to haze in the reaction scheme. This is particularly important for the chemistry of C₂H₂, the main hydrocarbon species from which the solid haze material is derived (Yung et al., 1984). However the chemical reactions that incorporate N into the haze have not yet been elucidated. McKay (1996) has shown that the C/N ratio of the starting mixture will alter the optical properties of tholin produced in that mixture. The reactions responsible for incorporating N-containing compounds into the haze may operate at different altitudes than those for C-containing compounds (Lara et al., 1999). Thus the C/N ratio, and presumably the optical properties of the haze, may vary with altitude (as suggested by Chassefière and Cabane, 1995). The ratio of C₂H₂ to HCN varies with latitude (Coustenis and Bézard, 1995). Since these molecules are

Table 2
Production rates of mass, N, and C (McKay, 1996)

Process	Mass ($\text{g cm}^{-2} \text{s}^{-1}$)	N ($\text{cm}^{-2} \text{s}^{-1}$)	C ($\text{cm}^{-2} \text{s}^{-1}$)	
C from CH_4 photolysis	2.6×10^{-13}	—	1.3×10^{10}	Toublanc et al. (1995)
N from N_2 dissociation	2.0×10^{-14}	8.4×10^8	—	Strobel et al. (1992)
Tholin production	10^{-14}	1×10^8	4×10^8	Toublanc et al. (1995) Assuming $\text{C}_4\text{H}_4\text{N}$ (C/N = 4)

Table 3
Estimates of Titan haze production rates

Citation	Rate ($10^{-14} \text{ g cm}^{-2} \text{ s}^{-1}$)	Note
<i>Pre-Voyager</i>		
Podolak and Bar-Nun (1979)	3.5	C_2H_4 , C_2H_2 , and CH_4 , photolysis
Toon et al. (1980)	35	Microphysical model in CH_4 matching albedo
<i>Voyager</i>		
Yung et al. (1984)	~ 2	Photochemical model, hydrocarbons only
McKay et al. (1989)	1.2	Simple microphysical model matching albedo
Samuelson and Mayo (1991)	0.8	Voyager thermal infrared spectra
Toon et al. (1992)	1.2	Wind and detailed microphysics model matching albedo
Thompson et al. (1994)	0.5–4	Laboratory simulations
Lara et al. (1994)	1.7	Photochemical model, hydrocarbons only
Rannou et al. (1995)	1.4–3.5	Fractal microphysics matching albedo
Rannou et al. (1997)	0.6	Fractal microphysics matching high phase angle photometry
Tomasko et al. (1997)	0.4	Spherical microphysical model
	1.5	Fractal microphysics model

likely to be the respective principal starting points for C and N incorporation into the haze, one might expect that the C/N ratio and optical properties of the haze will vary with season – a possibility suggested by Courtin (1992) to explain the seasonal brightness change of the haze. As argued above, particle density and size variations may also play a role in the hemispherical albedo asymmetry.

McKay (1996) reported the results of a study on the solubility of tholin in liquid ethane and found that tholin was insoluble at the level of measurement (0.03% by mass). Tests in a variety of solvents (McKay, 1996) revealed that tholin material is much more soluble in polar solvents (water, ethanol, methanol, glycol, and dimethylsulfoxide) than in non-polar solvents (ethane, hexane, benzene). This result is consistent with the theoretical work by Raulin (1987) if the tholins resemble polyacetylene or nitrogen-containing polymers and not polyethylene (Guez et al., 1997). As pointed out by McKay (1996) the insolubility of haze material in non-polar compounds could have implications for the condensation of ethane and methane in Titan's atmosphere. Coll et al. (1999) confirmed these results and also found that the tholin material was soluble in acetonitrile at levels of 0.4%, and in other nitriles as

well. Condensation may be inhibited or completely suppressed by the insolubility of the tholin and the resulting large contact angles between particle surfaces and condensing ethane and methane. Courtin et al. (1995) has suggested that this could result in supersaturations of ethane of over 500 in Titan's stratosphere and supersaturations of methane of over 2 in the troposphere.

4. Haze production rates and bulk optical properties

A variety of microphysics models have been developed to simulate the nature of the haze on Titan. Table 3 is a summary of the estimates in the reviewed literature of the production rate of haze in Titan's atmosphere. The first estimates of haze production made *before* the Voyager results were as follows: Podolak and Bar-Nun (1979) suggested a production rate of $3.5 \times 10^{-14} \text{ g cm}^{-2} \text{ s}^{-1}$ based on the rate of CH_4 photolysis as well as on the albedo required to match the observed reflectance of Titan; Toon et al. (1980), in a detailed microphysical model, found that a production rate of $35 \times 10^{-14} \text{ g cm}^{-2} \text{ s}^{-1}$ was needed to fit the geometric albedo in a pure CH_4 atmosphere.

After the Voyager encounter it was clear that the atmosphere of Titan was primarily N_2 , making the pre-Voyager estimates largely irrelevant. The detection of gaseous organics in the stratosphere confirmed that the haze was likely to be organic material. Yung et al. (1984) developed a photochemical model that, while giving only a perfunctory treatment of the chemistry of the C_n ($n > 4$) species, did include a series of reactions that produced hydrocarbon “polymer”. The net production of haze material in these reactions is given as $\sim 10^8$ molecules $cm^{-2} s^{-1}$. The mean molecular weight of the products of these reactions is approximately C_{10} , implying a mass production rate of $\sim 2 \times 10^{-14}$ g $cm^{-2} s^{-1}$. A similar approach was used by Lara et al. (1994).

McKay et al. (1989) used a simple monodisperse haze model based on the Voyager atmospheric profile to deduce that a haze production rate of 1.2×10^{-14} g $cm^{-2} s^{-1}$ would fit the geometric albedo from 0.3 to 2 μm . Samuelson and Mayo (1991) developed an estimate for the column mass of aerosol required to match the thermal infrared spectrum of Titan. From a simple estimate of the sedimentation velocity they determined a production rate of 0.8×10^{-14} g $cm^{-2} s^{-1}$. Toon et al. (1992), using a detailed aerosol model, found that a haze production rate of 1.2×10^{-14} g $cm^{-2} s^{-1}$ would fit the geometric albedo. Thompson et al. (1991) used a low pressure (0.24 mbar) plasma discharge to simulate radiation chemistry on Titan. Their published estimate for the production of solid organic material was from 0.3 to 3×10^{-14} g $cm^{-2} s^{-1}$, but in a subsequent publication they revised this to 0.5 – 4×10^{-14} g $cm^{-2} s^{-1}$ (Thompson et al., 1994), the values listed in Table 3. Rannou et al. (1995, 1997) and Tomasko et al. (1997) have considered the effects of fractal geometry on the haze. Although the dynamics of the haze is quite different with fractal shapes, the inferred production rates are similar to those obtained previously.

All the haze models listed in Table 3, from McKay et al. (1989) onward, have achieved a good fit to the spectral dependence of Titan’s geometric albedo by using modifications of the optical constants of Titan tholin material produced in the laboratory (Khare et al., 1984). McKay et al. (1989) reported that the best fit was obtained if the laboratory values for absorbance are multiplied by a factor of 4/3; this is shown in Fig. 4. Toon et al. (1992) found that a factor of 1.5 provided that best overall fit, while Rannou et al. (1995) found a factor of 3 in the UV and 1.5 in the visible. The sharp drop ($n_i \propto \lambda^{-4}$) in absorption from 0.3 to 0.9 μm in the tholin spectra is essential for reproducing the shape of Titan’s geometric albedo (McKay and Toon, 1992). Other materials such as poly-HCN which do not have this sharp drop (Khare et al., 1984) cannot match the albedo of Titan.

The geometric albedo of Titan is determined by the properties of the main haze layer. The optically thin detached haze layer occurring at high elevations above the main haze layer could well have different optical proper-

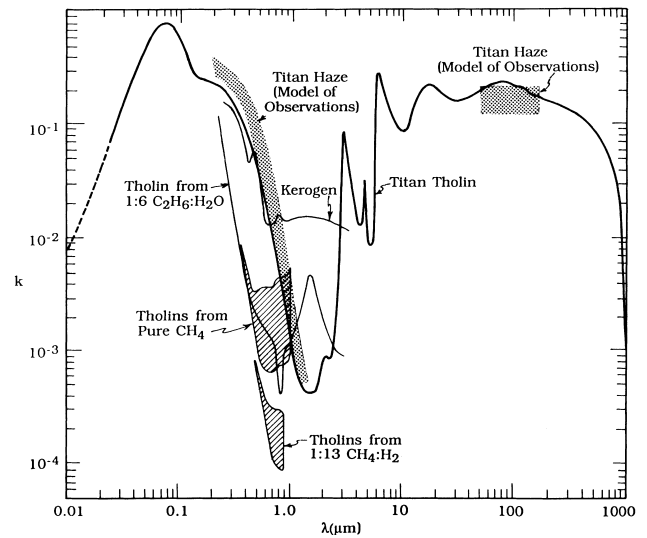


Fig. 4. Optical properties of Titan tholin produced from a 10% CH_4 –90% N_2 mixture, compared with other organic material. Shown by the dark regions are the optical constants inferred by McKay et al. (1989) that are required to match the geometric albedo in the visible simultaneously with the continuum emission in the thermal infrared (Sagan et al., 1992).

ties than the main haze. In fact in Voyager images the detached haze appears to have different optical properties than the main haze.

It is interesting to note that modeling of the thermal infrared emissions of Titan measured by Voyager can be used to determine the optical constants at these wavelengths as well (also shown in Fig. 4). Because the particles are small compared to thermal wavelengths, the haze opacity in the thermal infrared depends on the volume of haze material times the absorption coefficient. If the production rate in the haze model is constrained by fitting the geometric albedo in the visible, it is then possible to determine the absolute value for the haze absorption in the thermal infrared. This only works by considering the visible and thermal spectra together. Following this approach, McKay et al. (1989) determined that the optical properties of Titan tholin in the thermal infrared were equal to the laboratory values multiplied by a factor of $\sim 1/2$ (McKay et al., 1989). Courtin et al. (1995), using the haze model of McKay et al. with a more accurate computation of collision induced absorption, found that the scaling factor was between 0.3 and 0.8. Samuelson and Mayo (1991), from their analysis of the haze in the north polar region of Titan, were able to determine that in the thermal infrared the wavelength dependence of the haze was similar to that of laboratory tholin although they did not determine an absolute scale factor.

It is important to note that the haze production rate determined from the geometric albedo and the inference that the optical properties are similar to those of laboratory tholin are related. The production rate and tholin scaling factor are determined simultaneously by fitting the

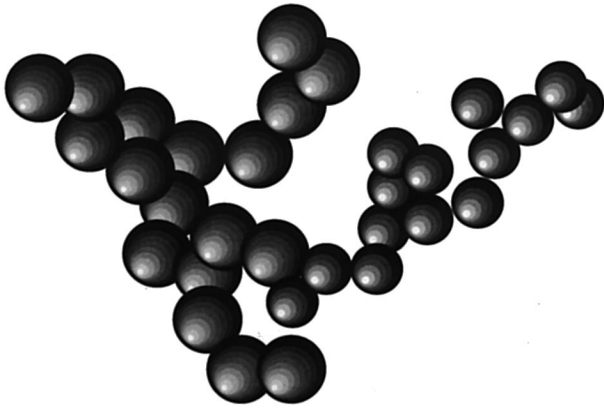


Fig. 5. Aggregate particle which may be typical of Titan's haze layer, formed with 32 monomers.

Table 4
Fractal dimension for different aggregation modes (Cabane et al., 1993)

Growth model of the cluster	Mean free path < radius	Mean free path > radius
Particles combining with clusters	2.5	3
Clusters combining with clusters	1.75	2

geometric albedo. There is remarkable agreement between the optical constants of laboratory tholin determined by Khare et al. (1984) and the microphysical models. It would be very useful to verify that laboratory tholin is indeed a good optical, and presumably therefore chemical and organic analogue to Titan haze. Thus other groups using other simulation methods should confirm the synthesis and the optical characterization of laboratory tholin produced in simulated Titan atmospheres (i.e. using CH_4 and N_2).

5. Fractal models and scattering properties of the haze

As discussed above, it is now thought that the particles in Titan's main haze layer are non-spherical aggregates. West and Smith (1991) first suggested aggregates of spherical "monomers" for Titan's haze. In a series of papers Cabane and coworkers (Israel et al., 1991; Cabane et al., 1992, 1993, 1995; Cabane and Chassefière, 1993, 1995; Rannou et al., 1993, 1995, 1997) have developed a sophisticated model of Titan's haze as fractal particles. A similar model has been developed by Tomasko et al. (1997). An aggregate particle is shown in Fig. 5.

The basis for fractal models lies in the observation that when liquid particles combine they form a new compact sphere corresponding to the combined mass, but when solid particles combine they can form a range of shapes from compact spheres to long strings of particles. A convenient parameter that characterizes the shape of these aggregates is the fractal dimension, D_f . Table 4, adapted from Cabane et al. (1993), gives the fractal dimension as a function of the aggregation conditions in Titan's atmosphere. When

monomers diffuse directly onto aggregates, building the aggregates one monomer at a time, the fractal dimension is 2.5 provided the mean free path is small. Where the mean free path is large and the monomers follow ballistic trajectories, the fractal dimension is 3 and compact spheres result, similar to liquid particles. If growth of the aerosols is dominated by aggregates combining with other aggregates, the fractal dimension is 1.75 if the mean free path is smaller than the particles, and 2 if it is larger.

Microphysical models (Cabane et al., 1992, 1993; Tomasko et al., 1997) suggest that Titan's main haze can be physically divided into two regions, a high altitude region in which the fractal dimension is 3 (monomer growth) and a lower altitude region in which the fractal dimension is 2 (cluster-cluster ballistic growth). Typical profiles for the haze particle sizes and densities are shown in Fig. 6 from Tomasko et al. (1997).

This can be understood following Cabane et al. (1992). Consider a photochemically active zone, located at altitude z_0 , assumed to be Gaussian as a function of the altitude z ($\Delta z_0 \sim 20$ km, such that this zone extends ~ 1 or 2 scale heights). At each instant the haze contains freshly produced macromolecules and larger, older particles. Since the coagulation process between particles is more efficient if the particles are of different size, continuous growth of the largest particles in the photochemical zone is promoted. These growing particles, roughly spherical in shape and compact (caused by the ballistic particle-cluster process, with a fractal dimension of $D_f = 3$), evolve into the monomers which will later build the aggregates. This hypothesis, originally derived from an Eulerian microphysical model of the aerosols (Israel et al., 1991), is confirmed when a given particle is followed in the course of its growth (Rannou et al., 1993). Schematically, the newly produced macromolecule undergoes some collisions with very small molecular clusters, but then quickly collides (within $\sim 10^4$ s) with a larger particle already present. These large particles continue to grow into a spherical shape (monomer) by accretion of macromolecules or small clusters (Rannou et al., 1993).

Once these monomers are sufficiently heavy they begin to fall out of the photochemical zone. The microphysical parameters z_0 (altitude of the photochemically active zone) and Q (photochemical production rate) may then be used to compute the size of the monomers. For $Q = 3.5 \times 10^{-14} \text{ g cm}^{-2} \text{ s}^{-1}$, and for altitudes $z_0 = 300, 385, 535$, and 680 km, the monomer radii are respectively $r_m = 0.13, 0.09, 0.03$, and $0.01 \mu\text{m}$. From this, one may deduce that a rather low production altitude, below 450 km, leads to monomer radii consistent with the optical properties of Titan's atmosphere (Rannou et al., 1995). Below the photochemical zone, the collisions occur without the presence of smaller particles, since these latter are incorporated into the monomers faster than they settle.

As the particles fall to lower altitudes, the coagulation process occurs between clusters formed from the

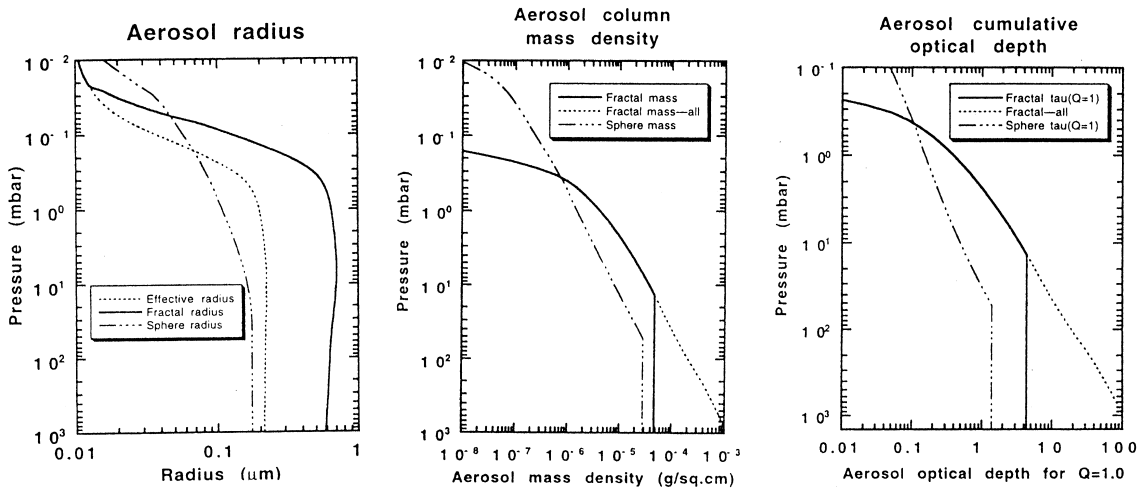


Fig. 6. Profiles of haze properties from the spherical and fractal microphysical models of Tomasko et al. (1997). Panel (a), aerosol size. The heavy solid line shows the fractal radius (approximately the radius of gyration). The dashed line corresponds to the radius of an equivalent volume sphere. The dotted-dashed line shows the mean radius for a spherical drop model. Panel (b), column mass density. The solid line is the cumulative mass. Note the break at 10 mbar resulting from rainout removal. The dotted-dashed line shows the result for a spherical drop model. Panel (c), geometric optical depth. The total column particle cross-section for the fractal case with rainout removal (solid), without rainout removal (dotted) and for the spherical drop model (dotted-dashed). The optical depth at any given wavelength would be the column geometric optical depth times the efficiency factor.

aggregation of monomers. The atmospheric pressure is sufficiently low to allow us to assume that the coagulation processes are again ballistic so that the fractal dimension of the aggregates is $D_f \sim 2$ (Table 4). Due to fractal auto-similarity, D_f is preserved down through the stratosphere. If condensation of hydrocarbons begins to occur on the haze particles (~ 80 km), then the average size of an aggregate increases as each monomer grows. Adapting their microphysical modeling (including settling, coagulation, etc.) to the fractal hypothesis, Cabane et al. (1993) compute the distribution of fractal particles at any altitude level, from which they deduce the average number of monomers in the fluffy aggregates at a given level z . For a given set of parameters, z_0 and Q , one observes, at first, a rapid increase in the number of monomers in the aggregates. Then, below ~ 200 km, the number remains almost constant. For $Q = 3.5 \times 10^{-14} \text{ g cm}^{-2} \text{ s}^{-1}$, and production altitudes of $z_0 = 385$ and 535 km, the maximum values of the number of monomers are, respectively, ~ 18 and 700 ; corresponding “radii” for fluffy aggregates are ~ 0.5 and $1.0 \mu\text{m}$ respectively. For the same microphysical conditions, liquid-drop radii would be $\sim 0.2 \mu\text{m}$ in both cases (Cabane et al., 1993).

It had been recognized earlier that a bimodal distribution was necessary to explain the optical properties of Titan’s atmosphere (Tomasko and Smith, 1982; Courtin et al., 1991; Toon et al., 1992). Fractal models of a haze composed of monomers in the upper altitudes and fractals in the lower layer effectively respond like a bimodal distribution of particles. The small particles, both the free monomers and the monomers within aggregates, interact with short wavelength radiation and also determine the

polarization. Thus the UV and polarization data can be explained. At longer wavelengths the aggregates behave like large particles and can reproduce the geometric albedo and forward scattering properties observed for Titan (Rannou et al., 1997). In addition, as discussed above, fractal particles seem to better fit the limb data results of Karkoschka and Lorenz (1997) associated with Titan’s shadow on Saturn. In this study, absorption at short wavelengths (~ 337 nm) appears to be too large to be consistent with spherical particles of one size.

The optical properties of a fractal particle differ from those of a sphere of equivalent mass or area in the sense that, in the fractal case, one has to deal with the interactions of fields radiated by each of the monomers of the aggregate (West, 1991). Rannou et al. (1997) has developed a treatment which considers the monomers within each aggregate using Mie theory with the simplifying assumption that the radiation field within the aggregate itself is uniform (the mean field approximation). Computationally rapid schemes have also been developed (Mackowski and Mishchenko, 1996; Rannou et al., 1999). Once the optical properties (phase function, cross sections, etc.) of a given particle are known, radiative transfer solutions for Titan’s atmosphere may be computed and, after comparison with observational results, can be used to determine the production rate (see Table 3), altitude, and optical properties of the haze material. A comparison of the geometric albedo computed with the fractal model (Rannou et al., 1995) and the spherical model (McKay et al., 1989) is shown in Fig. 7. As can be seen, the low UV albedo that results from many small monomers is reproduced in the fractal model. The values of the absorption index of the haze,

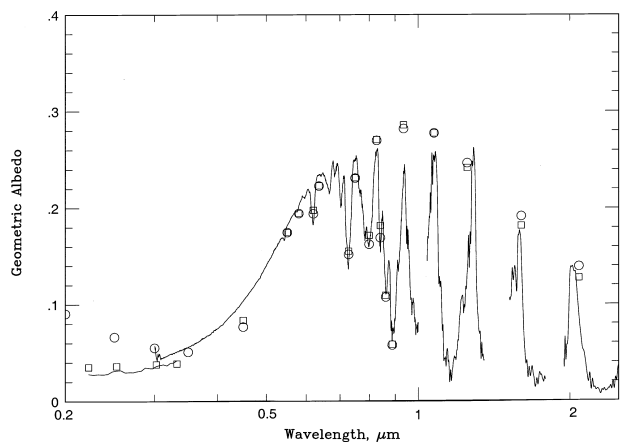


Fig. 7. Geometric albedo of haze with fractal and spherical particles compared. Solid line is the data from Fig. 1, squares are the fractal model (Rannou et al., 1995) and circles are the spherical model (McKay et al., 1989).

obtained from the fractal model, are comparable to but higher than the experimental values (Khare et al., 1984) obtained from terrestrial analogous (factor of ~ 3 in the UV and ~ 1.5 in the visible), although they do follow the same variation with wavelength (Rannou et al., 1995).

The fractal model of the aerosols has also been applied by Rannou et al. (1997) to calculations of limb profiles at phase angles of 140° and 155° , as observed by Voyager (Rages and Pollack, 1983); here again the method leads to a good fit with the observations. The intensity profiles are consistent with haze production at low altitude ($z \leq 385$ km), while the production rate and absorption index of the haze are consistent with previous values (Rannou et al., 1997). The fractal model was also used by Coustensis et al. (2000b) to infer the Titan infrared surface albedo.

6. Thermal and dynamic interactions with haze

Our understanding of the interrelations that exist between Titan's haze and motions in the atmosphere is at present quite limited. What is known to date is more adapted to suggesting the types of questions to ask of future data (e.g. data to be acquired from the Cassini mission) than it is to determining solutions from existing data. Even so, certain general statements and speculations can be made at present regarding both the effect of haze on atmospheric dynamics, and conversely, the question of how motions of the atmosphere are manifested in the appearance of the haze.

The fundamental way in which haze particles influence atmospheric motions is through the absorption and redistribution of radiant energy. Solar radiation is absorbed by the particles and converted into atmospheric thermal energy. Conduction of heat from haze particles to the surrounding gas is efficient enough to maintain the particles to within a few hundredths of a kelvin of the gas temperature (Samuel-

son, 1970). The atmospheric thermal gradients established are modified by heating and cooling by the infrared radiation field, and ultimately become responsible for motions that attempt to bring the atmosphere back into thermal and dynamic equilibrium.

The haze interacts strongly with sunlight in the upper atmosphere of Titan, reflecting 30% and absorbing 40% of the incident sunlight (McKay et al., 1991), thus being the dominant mechanism for producing the high temperatures and thermal gradients in Titan's stratosphere (see Hanel et al. (1992) for a comparison with other planets in the solar system). Since the haze has very low optical depth in the thermal infrared it allows thermal energy to escape readily even as it blocks the penetration of sunlight. This leads to an antigreenhouse effect (McKay et al., 1991), so-called because it is responsible for cooling the surface of Titan by 9 K compared with what the surface temperature would be if the haze were absent. On the other hand the infrared opacity of the troposphere acts as a thermal blanket (the greenhouse effect), warming the surface of Titan by 20 K compared with what it would be in the absence of a troposphere. The surface thus becomes a net 11 K warmer than its equilibrium temperature of 84 K.

Radiative response times are much longer in the lower troposphere (Smith et al., 1981) and much shorter in the mid- and upper-stratosphere (Flasar et al., 1981) than the length of Titan's seasonal cycle (29.5 yr). If only radiative effects determined the thermal structure, the latitudinal variation of temperature would reduce to the seasonal average in the troposphere, whereas it would follow the sun in the upper stratosphere. Thus, temperatures should exhibit latitudinal symmetry in the troposphere and depend on season in the stratosphere.

Qualitatively, the former situation is consistent with the 2–3 K reduction in surface temperature at high latitudes in both hemispheres (compared with those near the equator) found by Flasar et al. (1981) and Samuelson et al. (1997b). According to Flasar et al. (1981), however, the expected radiative equilibrium surface temperature difference between equator and high latitudes is ~ 15 K, implying that dynamical transport of heat is required in the troposphere to reduce this difference to the amount observed. One mechanism for transporting heat latitudinally is by baroclinic waves. According to Leovy and Pollack (1973), the fastest growing baroclinic waves (associated e.g. with weather systems) have length scales larger than the radius of Titan if the vertical lapse rate is close to adiabatic. This suggests that baroclinic waves are not likely to be effective in transporting heat in Titan's troposphere. Flasar et al. (1981) point out that the observed lapse rate is distinctly subadiabatic throughout most of the troposphere, leading to increased static stability and thus to a preferred scale of eddies that is even longer, reinforcing the argument of Leovy and Pollack.

An alternative heat transfer mechanism is one that produces zonally symmetric meridional circulations (Hadley

cells). In the troposphere, warm air rises at the equator and subsides at high latitudes, transporting heat poleward and reducing latitudinal temperature gradients in the process. Because these gradients are only reduced and not eliminated, however, the thermal wind equation requires that zonal wind velocities increase with altitude, beginning with zero velocity at the surface. The steady monotonic decrease of surface temperature with increasing latitude in the troposphere suggests that horizontal gradients of the zonal winds will tend not to fluctuate frequently with changing latitude.

The situation is somewhat different in the stratosphere. Because of the short radiative response time to the sun, the latitudinal temperature field will vary asymmetrically with the season. If the opacity were independent of latitude and dynamics were unimportant, the temperature field in the upper stratosphere would be symmetric about the equator at the equinoxes, and most asymmetric about the equator at the solstices. However, Flasar et al. (1981) showed from Voyager 1 IRIS data that stratospheric temperatures were highly asymmetric at northern vernal equinox, the time of the Voyager 1 flyby. This implies that either dynamics or an asymmetrically distributed opacity (or both) were affecting the temperature field at this time.

Bézar et al. (1995) examined the case of an asymmetrically distributed stratospheric opacity. They adopted the latitudinal abundances of the various hydrocarbons, nitriles, and haze determined by Coustenis and Bézar (1995) and calculated stratospheric heating and cooling rates based on these abundances. They then assumed that a state of radiative equilibrium existed, and inferred that the integrated ratio of infrared-to-visible absorption coefficients in the north was greater than that in the south by the amount required to account for the observed temperature differences.

Flasar and Conrath (1990) examined the dynamical implications of the observed latitudinal temperature asymmetry in the stratosphere. They pointed out that latitudinal temperature gradients were largest at northern high latitudes. Under these circumstances the thermal wind equation requires zonal wind velocities to be higher in the north than at comparable latitudes in the south. This in turn requires that angular momentum be transported from north to south as the season progresses and zonal velocities become more comparable. Such transport is accomplished by a meridional circulation pattern in which mass is transported from north to south in the top branch of the pattern. Rising air in the north will expand and cool, whereas subsiding air in the south will compress and heat. These adiabatic processes counteract efforts of the atmosphere to return to a state of radiative equilibrium, delaying thermal response to the sun. Flasar and Conrath inferred a dynamical relaxation time about a factor 5 greater than the corresponding radiative relaxation time, which could account for the apparent phase lag of the stratospheric temperature field with respect to the sun

of about one season. A detailed account of the process is given by Flasar (1998b).

Two sets of observations suggest global cyclostrophic wind fields for Titan's upper atmosphere. Sicardy et al. (1990) and Hubbard et al. (1993) observed the 1989 occultation by Titan of the star 28 Sgr, and concluded from analyses of the central flash that Titan's atmosphere had an equatorial bulge that would be consistent with high-speed equatorial zonal winds. Kostiuik et al. (1997) inferred prograde wind speeds of $\sim 70 \text{ m s}^{-1}$ (with a large uncertainty) from Doppler heterodyne spectroscopy of stratospheric ethane emission lines.

Progress toward understanding the dynamics of Titan's atmosphere has been advanced with the help of general circulation models (Del Genio et al., 1993; Hourdin et al., 1995; Tokano et al., 1999). Del Genio et al. (1993) investigated zonal winds with a general circulation model (GCM) designed for Earth, but with the length of day scaled to Venus and Titan values. Although they did not have correct heating rates in their model, they found that it was possible to generate high zonal winds in a cloudy atmosphere. If the atmosphere were clear, however, they found that zonal winds tended toward very low velocities at low latitudes. Del Genio et al. found that solar heating at the surface generated free convection throughout a large part of the troposphere, causing efficient vertical mixing of heat and momentum. Drag by the surface was effectively transmitted high into the atmosphere, strongly coupling the upper troposphere to the surface and inhibiting equatorial winds aloft. If clouds were introduced into the middle and upper troposphere, however, solar heating was significantly reduced at the surface. The troposphere became statically stable, thereby suppressing free convection and effectively decoupling the troposphere from the surface. Under these conditions it becomes possible to generate high zonal winds in the equatorial stratosphere.

Application of these concepts to Titan suggests that the haze may indirectly be responsible for the high equatorial zonal winds implied by the heterodyne spectroscopy and 28 Sgr occultation data. Haze opacity reduces solar heating at the surface to an amount below that needed to make the troposphere convective, except possibly for the first three or four kilometers (Samuelson, 1983; McKay et al., 1989) (see also McKay et al., 1997). This tends to mechanically decouple the troposphere from the surface, and equatorial superrotation is no longer suppressed by strong drag forces. Of course some frictional coupling is required or no vertical wind gradients could be generated in the first place.

Hourdin et al. (1995) developed a detailed GCM designed specifically for Titan and found that starting from a state of rest the simulation spontaneously produced a strong superrotation with prograde winds reaching 100 m s^{-1} near the 1 mb level, in general agreement with the Del Genio et al. model containing clouds. Of course Titan's haze is implicitly built into the Hourdin

et al. model. They also inferred that the annually and seasonally averaged meridional circulation is dominated by large equator-to-pole Hadley cells. While a static (no dynamics) computation of temperatures produced results that agreed with the observations of Flasar et al. (1981), with dynamics included the computed temperature contrast was subdued and no longer matched the observations. Hourdin et al. (1995) suggest that this could be the result of keeping the haze and gas opacity constant in their simulation.

Tokano et al. (1999) found that varying the number density of the haze only could produce the observed temperature contrast but the variation was not consistent with the seasonal cycle of Titan's reflectivity. Their best fit to the temperature gradient was obtained when artificial damping is added to the model and the heating determined from a seasonally varying haze and with modified cooling rates to account for the enhancement of nitriles and hydrocarbons after vernal equinox.

Certain observational complications intrude into our simple picture of zonal winds as they apply to Titan. Voyager 1 and 2 images (Smith et al., 1981, 1982) show a faint, banded structure in the northern hemisphere, possibly implying that latitudinal perturbations to the zonal wind field occur in the stratosphere. Smith et al. (1982) plotted Titan's albedo variation with latitude, clearly showing several changes in albedo gradient with latitude. Because baroclinic eddies should be suppressed throughout Titan's atmosphere (e.g. Leovy and Pollack, 1973), it is unclear what transient phenomena give rise to the perturbations leading to these changing gradients.

The large-scale dynamical interaction between the haze and the atmosphere supporting it is demonstrated by the time-evolving albedo asymmetry between the two hemispheres. As the sub-solar point moves north and south over a Titan year, due to the 26.4° obliquity of the saturnian system, Titan's atmosphere responds with seasonal changes in haze opacity and/or particle scattering properties. This asymmetry is shown in Fig. 2. These changes act in consonance with changes in the latitudinal thermal structure in the sense that they also appear to lag the solar forcing by about 90° of phase. When the sunlight on each hemisphere is about the same (at the equinoxes in 1980 and 1995, for example), the albedo contrast between the northern and southern hemispheres is at its strongest. No spatially resolved data exist for Titan near solstice, although the disk-integrated albedo (which varies sinusoidally with a period of about 15 yr) is compatible with the hemispheres being about the same brightness during solstice. The Infrared Space Observatory (ISO) data taken in 1997 show atmospheric abundances on the order of what was found near Titan's equator in 1980 from Voyager IRIS data (Coustenis et al., 2000c). This is reasonable if the north–south asymmetry on Titan was reversed as expected from seasonal effects. The north–south asymmetry is discussed in detail in Sromovsky et al. (1981) and Lorenz et al. (1997).

It is believed (Hutzell et al., 1993) that changes only in the photochemical production of aerosols cannot be responsible for the albedo variation and the north–south albedo asymmetry, as the time constants associated with the aerosol formation and accumulation into optically thick layers are much longer than the seasonal period. Some success has been achieved in controlling the haze abundance by applying a Hadley cell type circulation to a model of Titan's aerosols (Hutzell et al., 1996), though inconsistencies remain and further work is needed. Changes in optical properties and particle composition may occur as a result of condensation of trace gases, as well as changes in the interacting gas composition due to varying photochemical production and destruction rates during the course of the year (Courtin et al., 1991). Hourdin et al. (1995) have generated a GCM model for Titan with a fixed haze structure – a next step is to model the response to a varying haze structure.

Lorenz et al. (1997) have suggested that the amplitude of the north–south albedo contrast cycle may be asymmetric – i.e., the bright/dark albedo ratio at northern spring equinox may be larger than that at northern autumn equinox. This asymmetry may be an effect of Saturn's eccentric orbit around the sun, and the fact that perihelion occurs close to southern summer solstice. Thus the daily-averaged peak insolation is higher at the south pole (7.4 W m^{-2}) than at the north pole (about 6 W m^{-2}) during their respective summers. The GCM model of Hourdin et al. (1995) indicates that during solstice there is a pole-to-pole Hadley-type circulation, rising in the summer hemisphere. The work by Hutzell et al. (1996) suggests that such circulation would transport small (dark) aerosols to the winter pole. Possibly the strength of the circulation (and perhaps also the amount of transported aerosol) would correlate with the intensity of the solar flux on the illuminated (summer) pole.

It should be remembered, however that the cross-equatorial circulation predicted by Hourdin et al. tends to require upwelling in the warmer hemisphere and subsidence in the colder, whereas that of Flasar and Conrath tends to flow in the opposite direction. Circulation is thermally forced in the former case, and mechanically forced in the latter. The model of Flasar and Conrath is incomplete in the sense that the forcing function is not specified. The model of Hourdin et al. is incomplete in the sense that the mechanical effects of propagating waves, important in the Earth's stratosphere, are not explicitly included (Flasar, 1998b). It becomes extremely important to determine the actual circulation observationally in order to infer which forcing function is dominant.

7. Condensation and precipitation

Various infrared spectra of Titan's north polar region obtained during the Voyager 1 flyby showed stratospheric emission features that could not be attributed to molecules in the vapor phase. The feature at 478 cm^{-1} was eventu-

ally identified as the ν_8 band of condensed dicyanoacetylene (C_4N_2) by Khanna et al. (1987). Other plausible candidates implied by the Voyager spectra include condensed HCN, HC_3N , C_2H_2 , C_2H_6 and CH_3CH_2CN (propionitrile) (Coustenis et al., 1999).

If seed nuclei are present to promote condensation, most of the organics found in Titan's stratosphere should condense (Maguire et al., 1981; Sagan and Thompson, 1984). C_2H_4 may be an exception. As discussed before, the photochemical aerosol present is probably not soluble in condensed non-polar hydrocarbons, such as CH_4 and C_2H_6 (Raulin, 1987; McKay, 1996), and this may be a factor, among other factors, that controls condensation efficiency.

On the other hand, Raulin (1987) suggested that the aerosol might be slightly soluble in condensed nitriles. Thus, the photochemical aerosol may be the source of seed nuclei for the condensed C_4N_2 found in the north polar hood. According to Samuelson et al. (1997a), the abundance of condensed C_4N_2 , inferred from its band at 478 cm^{-1} , is about two orders of magnitude greater at certain altitudes than would be possible if the C_4N_2 system were in a steady state. An upper limit of 4×10^{-10} for the vapor mole fraction of C_4N_2 in the stratosphere is inferred from the absence of the 471 cm^{-1} band (associated with its vapor phase) in the IRIS spectra. This upper limit yields a C_4N_2 saturation vapor pressure at 90 km; hence C_4N_2 condensation is limited to altitudes below this level. If all the vapor below 90 km were to condense, the amount of condensate, at least at levels immediately below 90 km, would be substantially less than that inferred from the 478 cm^{-1} band.

One possible explanation is that the abundances of both C_4N_2 vapor and condensate vary with the season. Yung (1987) suggested there may be a build-up of vapor during the polar winter, when it is protected from photolytic decomposition while in the winter shadow. As spring approaches, two things occur: (1) the stratosphere becomes colder (Flasar and Conrath, 1990), which causes increased condensation at this time, and (2) the polar shadow recedes, which enhances photolysis and hence the decomposition of C_4N_2 vapor above the shadow. The combination of these two processes is thought to lead to an excess of condensate relative to the amount of vapor available under steady-state conditions. Particle sizes are inferred from the observed 478 cm^{-1} band shape to be $\sim 5\text{ }\mu\text{m}$ in radius. These size particles will precipitate out from the stratosphere in less than a year, which is short compared with the duration of the spring season (about 7.5 yr). Thus precipitation may occur for only a short time during polar spring.

Such particles may also act as seed nuclei for the ethane haze suspected of being the large-particle component of the north polar stratospheric continuum between 200 and 600 cm^{-1} (Mayo and Samuelson, 1996). This component appears to be located near the tropopause or slightly above, and has the scattering properties at thermal wavelengths of a thin cloud of condensed ethane particles with radii of 5–10 μm or so. Once these particles precipitate into the tro-

posphere, they in turn should act as seed nuclei for methane particles that condense there.

Before the Voyager missions, information about the troposphere of Titan was non-existent. IRIS spectra from the Voyager 1 encounter, coupled with radio occultation temperature profiles, permitted a determination of the tropospheric opacity between 200 and 600 cm^{-1} . Preliminary analysis by Courtin (1982) indicated that collision-induced absorptions from the various combinations of N_2 , CH_4 , and H_2 were insufficient to account for all the tropospheric opacity, and Samuelson et al. (1981) suggested that methane clouds might provide the remainder. This view was also adopted by Courtin (1982) and Thompson and Sagan (1984). It was implicitly assumed by the above workers that the absorption properties of liquid or solid methane defined the opacity properties of the methane cloud.

More extensive calculations were made by Toon et al. (1988), who used updated coefficients for collision-induced absorption and introduced multiple scattering into the radiative transfer calculations used to fit the IRIS data. They concluded that only very small or very large methane particles were consistent with the data. Submicrometer-size particles had the correct optical properties, but could be ruled out on physical grounds. Large numbers of very small particles do not provide a stable configuration – they would rapidly coagulate and grow. Also, optical cross-sections in the visible are orders of magnitude larger than in the thermal infrared for these particles, and solar radiation could not penetrate to the surface, thereby making it impossible to generate the observed greenhouse effect (McKay et al., 1989).

Instead, relatively small numbers of very large particles were advocated by Toon et al. (1988). They argued that the density of nucleation sites was considerably less on Titan than on the Earth, and that particles could grow to a larger size on Titan before exhausting the supersaturated vapor available for condensation. These larger particles would precipitate at a velocity large enough to accumulate smaller, slower particles rather quickly, and rapid growth would quickly lead to rain. Thus Toon et al. (1988) introduced the concept of “rain without clouds”. They suggested that instead of forming clouds per se, methane particles would grow directly into millimeter-size raindrops and quickly fall to the surface.

At this time inaccuracies still remained in calculating collision induced absorption coefficients to fit the gaseous contribution to the thermal continuum. Adequate data and procedures were finally obtained and developed in the late 1980s and early 1990s, however, especially in connection with CH_4 – CH_4 and N_2 – CH_4 pairs (see, e.g. Borysow and Frommhold, 1987; Birnbaum et al., 1993; Borysow and Tang, 1993). These studies led Courtin et al. (1995) and Samuelson et al. (1997b) to suggest large degrees of methane supersaturation in Titan's troposphere in order to account fully for the opacity between 200 and 600 cm^{-1} . This additional opacity replaced the need for opacity due

to methane clouds, although both Courtin et al. (1995) and Samuelson et al. (1997b) noted that thin ethane or methane clouds near the tropopause with particle radii $\sim 50\text{--}100\ \mu\text{m}$ were consistent with the data. Mayo and Samuelson (1996) noted that clouds with smaller particle radii ($\leq 10\ \mu\text{m}$) seemed to be required to fully explain the continuum opacity between 200 and $600\ \text{cm}^{-1}$ associated with the north polar hood. The ideas of Toon et al. (1988) about rain without clouds were put on a quantitative footing at this time by Samuelson and Mayo (1997), who developed a steady-state theory of methane condensation in Titan's troposphere in an effort to explain the high degrees of methane supersaturation found there.

An overview of one possible chain of events is as follows. C_4N_2 , which can act as a weak solvent for aerosol seed nuclei, freezes in the polar stratosphere (Samuelson et al., 1997a). Whether or not tholin-like particles can act as condensation nuclei is not clear. Some of the C_4N_2 ice particles (as well as those from other nitriles and possibly higher hydrocarbons) in turn act as seed nuclei for freezing C_2H_6 , the most abundant condensable in the lower stratosphere (Samuelson and Mayo, 1997). These particles grow to radii $\sim 10\ \mu\text{m}$ and precipitate into the upper troposphere where supersaturated methane freezes onto them. These new particles grow rapidly to radii of a few millimeters and fall to about the 12 km level where they melt. Internal dynamics stirs the liquid CH_4 and C_2H_6 into a homogeneous mixture. The individual particles then fall to near the surface where they evaporate almost but not quite completely. The remnants consist of uniformly mixed but ethane-enriched particles slightly larger than the original ethane seed nuclei. These particles produce a thin ground fog, individual particles of which eventually precipitate to the surface, providing an enrichment of liquid ethane there.

It is not clear if a similar situation occurs at low latitudes. Nitriles may not condense in the stratosphere, principally because photolysis inhibits their net production to below condensable amounts. If they do, the amount of condensate is not observable. As a consequence ethane will condense at a much reduced rate, if at all, and individual particles will be considerably larger. Also, stratospheric temperatures are considerably warmer at low latitudes compared with the spring pole, and condensation will generally be less likely if viable seed nuclei from other condensates are unavailable. Conservation of mass requires that the flux of precipitating ethane particles be inversely proportional to the cube of their mean terminal radius. Steady-state theory (Samuelson and Mayo, 1997) suggests that, globally, ethane seed nuclei with $r \sim 100\text{--}200\ \mu\text{m}$ or so are compatible with the degrees of methane supersaturation $S \sim 1.5\text{--}2.0$ found by Courtin et al. (1995) and Samuelson et al. (1997b). The accumulation and resulting enrichment of ethane on the surface will be much less at low latitudes than that at the poles because the downward flux of liquid ethane is less.

Conventionally, it has been assumed that aerosol particles descend through Titan's atmosphere until they reach

the upper stratosphere or the troposphere, where they act as nucleation sites for ethane or methane condensation, respectively, and are subsequently rained out onto the surface. The expected result is to clear the lower atmosphere of haze particles. However this may not be the case. First, methane or ethane may condense only on a limited subset of the aerosols falling through the saturated layer for either kinetic (Samuelson and Mayo, 1997; Guez et al., 1997) or chemical compatibility reasons (McKay, 1996). Second, Lorenz (1993) showed that falling raindrops consisting of pure methane would evaporate before they reached Titan's surface (unless the surface terrain is sufficiently elevated with respect to the locations on Titan where the Voyager radio occultation experiments took place). This would re-deposit aerosol particles at low, but non-zero altitudes in the troposphere, perhaps forming a haze. Thus, if ethane did not condense on the haze particles initially, there may well be some aerosol opacity in Titan's lower atmosphere, and determination of the haze concentration in this region of Titan's atmosphere would provide important information for use in haze microphysical and condensation cloud models.

Local transient phenomena cannot be ruled out. Evidence for occasional clouds in Titan's mid-troposphere has been obtained by Griffith et al. (1998), as discussed previously in Section 2.1. Awal and Lunine (1994) examined moist convection in Titan's atmosphere, and found that the maximum fractional areal coverage of Titan by convective plumes, if they exist, is very small ($< 10^{-5}$). Thus, clouds in Titan's troposphere may be intense but short-lived phenomena. Whether such occasional tropospheric clouds are physically compatible with a general state of high methane supersaturation has not yet been investigated.

8. Effects on the surface

The very presence (and mass) of Titan's atmosphere suggests that the evolution of the surface is closely coupled to that of the atmosphere. Unless replaced from below, stratospheric methane will be exhausted by photolytic destruction in \sim two million years (Lunine et al., 1983); (see also Flasar, 1998a). This implies that methane is being resupplied to the atmosphere from a surface reservoir. In turn, the continuous production of hydrocarbons and nitriles by methane photolysis, and their subsequent precipitation, must result in a net accumulation of these materials on the surface.

The most abundant photochemical by-product is ethane. As noted in Section 7, once formed, ethane will diffuse to the cold trap in the lower stratosphere, condense there, and precipitate to the surface. At prevailing temperatures, any condensed ethane at the surface will be in the liquid phase. Lunine et al. (1983) proposed that over the age of the solar system a large reservoir of liquid ethane will accumulate. The total amount may be expressed as an equivalent global ocean depth. Various models yield estimates for this depth – depending on the composition –

as ~ 600 m (Yung et al., 1984), ~ 200 m (Lara et al., 1994), and ~ 1000 m (Toublanc et al., 1995). Any actual reservoir formed this way may in fact contain up to ~ 15 times this value, as the “ocean” may also contain a significant fraction of liquid methane and nitrogen (Lunine et al., 1983; Lellouch et al., 1989; Dubouloz et al., 1989).

Sagan and Dermott (1982) gave theoretical arguments suggesting that any deep oceans on Titan would have to be global in extent. Continental structures similar to those of Earth would act to provide sufficient tidal friction to make Titan’s orbit around Saturn more circular than it presently is. On the other hand radar reflectivity measurements by Muhleman et al. (1990) are inconsistent with a global ocean, suggesting that Titan’s liquid inventory may have largely percolated downward into a porous regolith and become part of a deep subsurface reservoir, although lakes and limited small, shallow seas might still remain (Stevenson, 1992; Kossacki and Lorenz, 1995).

As described in Sections 2.1 and 2.2, near-IR spectroscopy and imaging suggest a heterogeneous surface. Topography on Titan is not well-constrained, but by analogy with other satellites, features of height ≤ 10 km might be expected. Such “mountains” would appear bright in the images and increase the surface albedo generally, because they tend to reduce methane vapor absorption above the surface and/or because methane rain has washed the higher areas clean of precipitating aerosol. Surface wind velocities are thought to be quite low due to high atmospheric density and small horizontal thermal gradients. Whether or not variable topography could induce observable dynamical effects higher up is not presently known. Calculations by Coustenis et al. (2000b) show that a mountain alone could not fully explain the albedo variations between Titan’s leading and trailing hemispheres. Some other bright component has to be present on the surface.

The observed spectral dependence of the surface albedo may help constrain the nature of any precipitates accumulating on the surface. Coustenis et al. (1995) have attempted to infer surface composition characteristics by observing in various spectral windows. Latest modeling efforts taking into account fractal particles (Coustenis et al., 2000b) indicate the surface albedo is a factor of two or more higher at 1.08, 1.28, and 1.6 μm than at 0.94 and 2.0 μm . This may be consistent with large areas of surface water ice covered with a more or less thick coating of tholin-like material.

9. Discussion and conclusions

A first-order description of Titan’s system of aerosols and clouds has been constructed over the last few decades from a wide variety of observations obtained by both ground-based and space-borne instruments. Some parts of the description are well defined; others are more hypothetical. Below we

outline our present understanding of the basic cycle through which Titan’s aerosol and cloud systems evolve.

Central to this understanding is the role that methane – presumably originating from an unspecified surface or subsurface reservoir – plays as the source of organic photochemistry in Titan’s atmosphere. Diffusion through the stratosphere and into the mesosphere and above places methane at altitudes where it can be dissociated by UV photolysis and charged particle bombardment. Molecular nitrogen dissociation also occurs high in the atmosphere. The dissociation products recombine to form simple nitriles and hydrocarbons, which diffuse downward into the stratosphere where additional chemistry takes place.

It is here, at altitudes of from 300 to 500 km, that Titan’s aerosol haze is formed. Initially, the haze particles grow as spheres (monomers) until their radii become ~ 0.1 μm ; in general a distribution of sizes is generated. The particles begin to fall, with different sizes falling at different velocities, resulting in frequent collisions and attendant coagulation. Aggregates of small spheres are formed, resulting in fractal particles that comprise the main haze on Titan.

Laboratory studies suggest these particles are refractory, consisting of simple alkanes, aromatics, and amino acid precursors. They appear to be insoluble in non-polar compounds such as ethane and methane, which suggests they may not serve as viable seed nuclei for condensation of these volatiles. This would account for the apparently high degree of methane supersaturation inferred for Titan’s troposphere. Possibly the haze particles are slightly soluble in nitriles, enabling them to act as condensation centers for the nitrile ices that form in the cold, polar stratospheric shadow during late winter and early spring. These ices in turn may act as condensation nuclei for stratospheric hydrocarbons, including ethane.

Independently of how they are formed, stratospheric ices will inevitably precipitate into the troposphere where they can serve as condensation nuclei for methane. Particle fluxes are too low, however, to reduce the globally averaged degree of methane supersaturation to the point where global cloud cover can be maintained. Instead, once formed, methane particles will on the average grow rapidly into hailstones, falling through the bulk of the atmosphere in less than two hours. When the hailstones reach an altitude of ~ 12 km they should melt, forming raindrops that may or may not fragment into smaller droplets, depending on whether or not they are too large to remain stable against turbulence generated by the slip-stream of air flowing past them.

Once they enter subsaturated air within a few kilometers of the surface, the raindrops and their fragments quickly evaporate to become small, stable particles highly enriched in ethane. These particles slowly settle to the surface to become part of the liquid reservoir from whence they originated. Over time the reservoir becomes depleted in methane and enriched in ethane and other hydrocarbons and nitriles. Because precipitation is less likely to occur in

regions exposed to constant sunlight, where the initial source is subject to photolysis, the liquid reservoir is likely to be less enriched by the higher organics at low latitudes than it is in the polar regions.

Within the context of this overall scenario, we can list some of the important physical properties of Titan's aerosol-cloud system:

1. Titan's haze is optically thick at visible wavelengths and has a detached upper layer. The hemispheric haze albedo goes through a seasonal cycle. Which hemisphere is brighter depends on wavelength (visible and near-infrared show opposite effects).
2. Microphysics models, photochemical models and laboratory simulations all suggest that the production rate of the haze is about $1 \times 10^{-14} \text{ g cm}^{-2} \text{ s}^{-1}$. Microphysics models imply that the total mass loading of the haze is about $2.5 \times 10^{-5} \text{ g cm}^{-2}$.
3. The optical depth at $0.5 \mu\text{m}$ is about 3, and thus about 10% of the sunlight reaches the surface.
4. At wavelengths above $1 \mu\text{m}$ the haze becomes increasingly transparent, both as a result of the change in the ratio of particle size to wavelength and because the absorption coefficient of the haze material becomes smaller.
5. The shape of the particles in the main haze deck is probably fractal (with fractal dimension 2) with an equivalent volume of a sphere of radius of $0.2 \mu\text{m}$.
6. The haze appears to be composed of organic material with a C/N ratio in the range 2–4, and a C/H ratio in the range 0.5–1.
7. Absorption of sunlight by the haze, which is relatively transparent in the thermal infrared, results in an anti-greenhouse effect which cools the surface by 9 K. The dominant source of heating in the stratosphere is the haze.
8. Stratospheric condensate clouds have been seen to date only near the local spring pole.
9. The only stratospheric condensate cloud component positively identified so far is C_4N_2 . The condensate abundance is about two orders of magnitude greater than permitted under steady-state conditions.
10. Tropospheric condensate clouds, if present, are thin, patchy, or transient. Under normal conditions methane hailstones may form and grow rapidly in a highly supersaturated environment, falling through most of the troposphere in less than two hours.

Key Questions about Titan's haze and clouds are:

1. What produces the detached haze at high altitude?
2. What is the cause of the seasonal variation? It is not production itself and appears to be related to dynamics.
3. Is the haze material at high altitude, particularly the detached haze layer, of different composition than lower

in the atmosphere? Are there seasonal changes in composition (e.g. does the C/N ratio vary with altitude and latitude)?

4. How is N incorporated into the haze?
5. What is the efficiency of haze particles as condensation nuclei for the various stratospheric hydrocarbons and nitriles and tropospheric methane?
6. Is the lower atmosphere cleared of haze by rainout?
7. Is there independent confirmation of the optical properties of tholin found by Khare et al. (1984)?
8. What are the compositions, altitudes, and particle sizes associated with stratospheric condensate clouds? At what latitudes are they located, and at what times of the year?
9. What are the frequency of occurrence, areal extent, and altitudes of tropospheric methane clouds?
10. What is the relationship between the existence of methane clouds and the degree of methane supersaturation?
11. And directly relevant to the upcoming Cassini mission and attempts to image the surface of Titan: what are the optical properties of the haze and any condensation clouds in the 1–3 μm range?

The Cassini orbiter and the Huygens probe will give considerable new information on Titan. On the probe, the Aerosol Collector Pyrolyser (Israel et al., 1997), in conjunction with the Gas Chromatograph-Mass Spectrometer instrument (Niemann et al., 1997) will analyze products from the thermal decomposition of the aerosols in Titan's atmosphere. Samples will be taken from 150 to 45 km and 30 to 15 km. The Descent Imager/Spectral Radiometer (Tomasko et al., 1997) will measure the solar aureole and the upward and downward radiative fluxes in the visible and IR. The Surface Science Package (Zarnecki et al., 1997) will study the surface state and composition at the landing site by measuring the speed of sound, the liquid density, the refractivity index, and liquid relative permittivity.

On the Cassini orbiter several instruments will provide information on the nature of aerosol and clouds during Titan flybys. The Imaging Science Subsystem (ISS) consists of a wide-angle camera with a 3.5° field of view, and a narrow-angle camera with a 0.35° field of view. The wide angle camera has eighteen filters covering the spectral range 380–1100 nm and the narrow angle camera has 24 filters covering the spectral range 200–1100 nm. The ISS will also obtain polarization data, useful in constraining haze and cloud particle properties. The Ultra-Violet Imaging Spectrometer will give information on the nature of the high-altitude haze. Observations by the Composite Infrared Spectrometer will enable determinations of organic molecules, haze opacity and cloud properties across latitude. Compositional information of both haze and clouds at high spatial resolution is potentially available from the spectra from the Visible and Infrared Mapping Spectrometer.

References

- Allen, D.A., Murdock, T.L., 1971. Infrared photometry of Saturn, Titan, and the rings. *Icarus* 14, 1–2.
- Awal, M., Lunine, J.I., 1994. Moist convective clouds in Titan's atmosphere. *Geophys. Res. Lett.* 21, 2491–2494.
- Bar-Nun, A., Kleinfeld, I., Ganor, E., 1988. Shape and optical properties of aerosols formed by photolysis of acetylene, ethylene and hydrogen cyanide. *J. Geophys. Res.* 93, 8383–8387.
- Bézard, B., Coustenis, A., McKay, C.P., 1995. Titan's stratospheric temperature asymmetry: a radiative origin? *Icarus* 113, 267–276.
- Birnbaum, G., Borysow, A., Buechele, A., 1993. Collision induced absorption of molecular gas mixtures: methane–nitrogen. *J. Chem. Phys.* 99, 495–510.
- Borysow, A., Frommhold, L., 1987. Collision induced roto-translational absorption spectra of CH₄–CH₄ pairs at temperatures of 50 to 300 K. *Astrophys. J.* 318, 940–943.
- Borysow, A., Tang, C., 1993. Far infrared CIA spectra of N₂–CH₄ pairs for modeling Titan's atmosphere. *Icarus* 105, 175–183.
- Cabane, M., Chassefière, E., 1993. Growth of aerosols in Titan's atmosphere and related time scales: a stochastic approach. *Geophys. Res. Lett.* 20, 967–970.
- Cabane, M., Chassefière, E., 1995. Laboratory simulations of Titan's atmosphere: organic gases and aerosols. *Planet. Space Sci.* 43, 47–65.
- Cabane, M., Chassefière, E., Botet, R., McKay, C.P., Courtin, R., 1995. Titan's geometric albedo: role of the fractal structure of the aerosols. *Icarus* 118, 355–372.
- Cabane, M., Chassefière, E., Israel, G., 1992. Formation and growth of photochemical aerosols in Titan's atmosphere. *Icarus* 96, 176–189.
- Cabane, M., Rannou, P., Chassefière, E., Israel, G., 1993. Fractal aggregates in Titan's atmosphere. *Planet. Space Sci.* 41, 257–267.
- Caldwell, J., Cunningham, C.C., Anthony, D., White, H.P., Groth, E.J., Hasan, H., Noll, K., Smith, P.H., Tomasko, M.G., Weaver, H.A., 1992. Titan: evidence for seasonal change — A comparison of Hubble Space Telescope and Voyager images. *Icarus* 97, 1–9.
- Chang, S., Scattergood, T., Aronowitz, S., Flores, J., 1979. Organic chemistry on Titan. *Rev. Geophys. Space Phys.* 17, 1923–1933.
- Chassefière, E., Cabane, M., 1995. Two formation regions for Titan's Hazes: indirect clues and hypothesized chemical synthesis processes. *Planet. Space Sci.* 43, 91–103.
- Clarke, D.W., Ferris, J.P., 1997. Titan haze: structure and properties of cyanoacetylene and cyanoacetylene–acetylene photopolymers. *Icarus* 127, 158–172.
- Coll, P., Coscia, D., Gazeau, M.-C., de Vanssay, E., Guillemin, J.C., Raulin, F., 1995. Organic chemistry in Titan's atmosphere: new data from laboratory simulations at low temperature. *Adv. Space Res.* 16 (2), 93–103.
- Coll, P., Coscia, D., Gazeau, M.-C., Guez, L., Raulin, F., 1998. Review and latest results of laboratory investigations of Titan's aerosols. *Origins Life Evol. Biosphere* 28, 195–213.
- Coll, P., Coscia, D., Smith, N., Gazeau, M.-C., Ramirez, S.I., Cernogora, G., Israël, G., Raulin, F., 1999. Experimental laboratory simulation of Titan's atmosphere: aerosols and gas phase. *Planet. Space Sci.* 47, 1331–1340.
- Combes, M., Vapillon, L., Gendron, E., Coustenis, A., Lai, O., Wittemberg, R., Sirdy, R., 1997. Spatially resolved images of Titan by means of adaptive optics. *Icarus* 129, 482–497.
- Courtin, R., 1982. The spectrum of Titan in the far-infrared and microwave regions. *Icarus* 51, 466–475.
- Courtin, R., 1992. Titan's UV albedo: Observations and modelling. In: Kaldeich, B. (Ed.), *Proceedings, symposium on Titan, ESA SP-338, European Space Agency Publications Division, Noordwijk*, pp. 59–67.
- Courtin, R., Gautier, D., McKay, C.P., 1995. Titan's thermal emission spectrum: Re-analysis of the Voyager infrared measurements. *Icarus* 114, 144–162.
- Courtin, R., Wagener, R., McKay, C.P., Caldwell, J., Fricke, K.-H., Raulin, F., Bruston, P., 1991. UV spectroscopy of Titan's atmosphere, planetary organic chemistry and prebiological synthesis. II. Interpretation of new IUE observations in the 220–335 nm range. *Icarus* 90, 43–56.
- Coustenis, A., Bézard, B., 1995. Titan's atmosphere from Voyager infrared observations. IV. Latitudinal variations of temperature and composition. *Icarus* 115, 126–140.
- Coustenis, A., Lellouch, E., Maillard, J.-P., McKay, C.P., 1995. Titan's surface: composition and variability from the near-infrared albedo. *Icarus* 118, 87–104.
- Coustenis, A., Salama, A., Lellouch, E., Encrenaz, Th., Bjoraker, G., Samuelson, R., de Graauw, Th., Feuchtgruber, H., Kessler, M.F., 1998. Evidence for water vapor in Titan's atmosphere from ISO/SWS data. *Astron. Astrophys.* 336, L85–L89.
- Coustenis, A., Schmitt, B., Khanna, R.K., Trotta, F., 1999. Plausible condensates in Titan's stratosphere from Voyager infrared data. *Planet. Space Sci.* 47, 1305–1329.
- Coustenis, A., Gendron, E., Lai, O., Veran, J.-P., Combes, M., Fusco, Th., 2000a. Adaptive optics images of Titan at 1.3 and 1.6 microns. Submitted for publication.
- Coustenis, A., Schmitt, B., Lellouch, E., McKay, C.P., Rannou, P., Cabane, M., Maillard, J.-P., Raynaud, E., 2000b. Titan's surface: monitoring and modeling from near-infrared spectra. Submitted for publication.
- Coustenis, A., Salama, A., Lellouch, E., Encrenaz, Th., Gautier, D., de Graauw, Th., Orton, G., Kessler, M. F., 2000c. Titan's mid-infrared spectrum from ISO observations. Submitted for publication.
- Danielson, R.E., Caldwell, J.J., Larach, D.R., 1973. An inversion in the atmosphere of Titan. *Icarus* 20, 437–443.
- Del Genio, A.D., Zhou, W., Eichler, T.P., 1993. Equatorial superrotation in a slowly rotating GCM: implications for Titan and Venus. *Icarus* 101, 1–17.
- Dubouloz, N., Raulin, F., Lellouch, E., Gautier, D., 1989. Titan's hypothesized ocean properties: the influence of surface temperature and atmospheric composition uncertainties. *Icarus* 82, 81–96.
- Flasar, F.M., 1998a. The composition of Titan's atmosphere: a meteorological perspective. *Planet. Space Sci.* 46, 1109–1124.
- Flasar, F.M., 1998b. The dynamical meteorology of Titan. *Planet. Space Sci.* 46, 1125–1147.
- Flasar, F.M., Conrath, B.J., 1990. Titan's stratospheric temperatures: a case for dynamical inertia?. *Icarus* 85, 346–354.
- Flasar, F.M., Samuelson, R.E., Conrath, B.J., 1981. Titan's atmosphere: temperature and dynamics. *Nature* 292, 693–698.
- Gibbard, S.E., Macintosh, B., Gavel, D., Max, C.E., de Pater, I., Ghez, A.M., Young, E.F., McKay, C.P., 1999. Titan: high resolution speckle images from the Keck telescope. *Icarus* 139, 189–201.
- Gillett, F.C., Forest, W.J., Merrill, K.M., 1973. 8–13 μm observations of Titan. *Astrophys. J. Lett.* 184, L93–L95.
- Griffith, C.A., 1993. Evidence for surface heterogeneity on Titan. *Nature* 364, 511–513.
- Griffith, C.A., Owen, T., Wagener, R., 1991. Titan's surface and troposphere, investigated with ground-based, near-infrared observations. *Icarus* 93, 362–378.
- Griffith, C.A., Owen, T., Miller, G.A., Geballe, T., 1998. Transient clouds in Titan's lower atmosphere. *Nature* 395, 575–578.
- Guez, L., Bruston, P., Raulin, F., Régnaut, C., 1997. Importance of phase changes in Titan's lower atmosphere. Tools for the study of nucleation. *Planet. Space Sci.* 45, 611–625.
- Hanel, R. et al., 1981. Infrared observations of the Saturnian system from Voyager 1. *Science* 212, 192–200.
- Hanel, R.A., Conrath, B.J., Jennings, D.E., Samuelson, R.E., 1992. *Exploration of the Solar System by Remote Infrared Sensing*. Cambridge University Press, Cambridge.
- Hinson, D.P., Tyler, G.L., 1983. Internal gravity in Titan's atmosphere observed by Voyager radio occultation. *Icarus* 54, 337–352.
- Hourdin, F., Talagrand, O., Sadourney, R., Courtin, R., Gautier, D., McKay, C.P., 1995. Numerical simulation of the general circulation of the atmosphere of Titan. *Icarus* 117, 358–374.

- Hubbard, W.B. et al., 1993. The occultation of 28 Sgr by Titan. *Astron. Astrophys.* 269, 541–563.
- Hunten, D.M., Tomasko, M.G., Flasar, F.M., Samuelson, R.E., Strobel, D.F., Stevenson, D.J., 1984. Titan. In: Gehrels, T., Matthews, M.S. (Eds.), *Saturn*. University of Arizona Press, Tucson, pp. 671–759.
- Hutzell, W.T., McKay, C.P., Toon, O.B., 1993. Effects of time-varying haze production on Titan's geometric albedo. *Icarus* 105, 162–174.
- Hutzell, W.T., McKay, C.P., Toon, O.B., Hourdin, F., 1996. Simulations of Titan's brightness by a two-dimensional haze model. *Icarus* 119, 112–129.
- Israel, G., Cabane, M., Raulin, F., Chassefière, E., Boon, J.J., 1991. Aerosols in Titan's atmosphere: models, sampling techniques and chemical analysis. *Ann. Geophys.* 9, 1–13.
- Israel, G. et al., 1997. The aerosol collector pyrolyser experiment for Huygens. In: Wilson, A. (Ed.), *Huygens: Science, Payload and Mission*, Vol. ESA-SP 1177, European Space Agency Publications Division, Noordwijk, pp. 59–84.
- Karkoschka, E., 1994. Spectrophotometry of the jovian planets and Titan at 300- to 1000-nm wavelength: the methane spectrum. *Icarus* 111, 174–192.
- Karkoschka, E., 1998. Methane, ammonia, and temperature measurements of the jovian planets and Titan from CCD-spectrophotometry. *Icarus* 133, 134–146.
- Karkoschka, E., Lorenz, R.D., 1997. Latitudinal variation of aerosol sizes inferred from Titan's shadow. *Icarus* 125, 369–379.
- Khanna, R.K., Perera-Jarmer, M.A., Ospina, M.J., 1987. Vibrational infrared and Raman spectra of dicyanoacetylene. *Spectrochim. Acta* 43A, 421–425.
- Khare, B.N., Sagan, C., 1973. Red clouds in reducing atmospheres. *Icarus* 20, 311–321.
- Khare, B.N., Sagan, C., Arakawa, E.T., Suits, F., Callcott, T.A., Williams, M.W., 1984. Optical constants of organic tholins produced in a simulated Titanian atmosphere: from soft X-ray to microwave frequencies. *Icarus* 60, 127–137.
- Khare, B.N., Sagan, C., Thompson, W.R., 1987. Solid hydrocarbon aerosols produced in simulated uranian and neptunian stratospheres. *J. Geophys. Res.* 92, 15,067–15,082.
- Kossacki, K.J., Lorenz, R.D., 1995. Hiding Titan's ocean: densification and hydrocarbon transport in an icy regolith. *Planet. Space Sci.* 44, 1029–1037.
- Kuiper, G.P., 1944. Titan: a satellite with an atmosphere. *Astrophys. J.* 100, 378–383.
- Kunde, V.G., Aikin, A.C., Hanel, R.A., Jennings, D.E., Maguire, W.C., Samuelson, R.E., 1981. C_4H_2 , HC_3N , and C_2N_2 in Titan's atmosphere. *Nature* 292, 686–688.
- Lara, L.M., Lorenz, R.D., Rodrigo, R., 1994. Liquids and solids on the surface of Titan. *Planet. Space Sci.* 42, 5–14.
- Lara, L.M., Lellouch, E., Lopez-Moreno, J.J., Rodrigo, R., 1996. Vertical distribution of Titan's atmospheric neutral constituents. *J. Geophys. Res. — Planets* 101, 23,261–23,283.
- Lara, L.M., Lellouch, E., Schematovich, V., 1999. Titan's atmospheric haze: the case for HCN incorporation. *Astron. Astrophys.* 341, 312–317.
- Lellouch, E., Coustenis, A., Gautier, D., Raulin, F., Dubouloz, N., Frère, C., 1989. Titan's atmosphere and hypothesized ocean: a reanalysis of the Voyager 1 radio-occultation and IRIS 7.7 μm data. *Icarus* 79, 328–349.
- Lemmon, M.T., Karkoschka, E., Tomasko, M., 1993. Titan's rotation: surface feature observed. *Icarus* 103, 329–332.
- Lemmon, M.T., Karkoschka, E., Tomasko, M., 1995. Titan's rotational lightcurve. *Icarus* 113, 27–38.
- Leovy, C.B., Pollack, J.B., 1973. A first look at atmospheric dynamics and temperature variations on Titan. *Icarus* 19, 195–201.
- Lindal, G.F., Wood, G.E., Hotz, H.B., Sweetnam, D.N., Eshelman, V.R., Tyler, G.L., 1983. The atmosphere of Titan: an analysis of the Voyager 1 radio-occultation measurements. *Icarus* 53, 348–363.
- Lockwood, G.W., 1977. Secular brightness increases of Titan, Uranus, and Neptune, 1972–1976. *Icarus* 32, 413–430.
- Lockwood, G.W., Thompson, D.T., 1979. A relationship between solar activity and planetary albedos. *Nature* 280, 43–45.
- Lockwood, G.W., Lutz, B.L., Thompson, D.T., Bus, E.S., 1986. The albedo of Titan. *Astrophys. J.* 303, 511–520.
- Lorenz, R.D., 1993. The life, death and afterlife of a raindrop on Titan. *Planet. Space Sci.* 41, 647–655.
- Lorenz, R.D., Lemmon, M.T., Smith, P.H., Lockwood, G.W., 1999. Seasonal change on Titan observed with the Hubble Space Telescope WFPC-2. *Icarus* 142, 391–401.
- Lorenz, R.D., Smith, P.H., Lemmon, M.T., Karkoschka, E., Caldwell, J., Lockwood, G.W., 1997. Titan's north-south asymmetry from HST and Voyager imaging: comparison with models and groundbased photometry. *Icarus* 127, 173–189.
- Low, F.J., 1965. Planetary radiation at infrared and millimeter wavelengths. *Lowell Obs. Bull.* 6, 184–187.
- Lunine, J.I., Stevenson, D.J., Yung, Y.L., 1983. Ethane ocean on Titan. *Science* 222, 1229–1230.
- Lutz, B.L., de Bergh, C., Owen, T., 1983. Titan: discovery of carbon monoxide in its atmosphere. *Science* 220, 1374–1375.
- Mackowski, D.W., Mishchenko, M.I., 1996. Calculation of the T matrix and the scattering matrix for ensembles of spheres. *J. Opt. Soc. Am. A - Opt. Image Sci. Vision* 13, 2266–2278.
- Maguire, W.C., Hanel, R.A., Jennings, D.E., Kunde, V.G., Samuelson, R.E., 1981. C_3H_8 and C_3H_4 in Titan's atmosphere. *Nature* 292, 683–686.
- McGrath, M., Courtin, R., Smith, T.E., Feldman, P.D., Strobel, D.F., 1998. The Ultraviolet albedo of Titan. *Icarus* 131, 382–392.
- McKay, C.P., 1996. Elemental composition, solubility and optical properties of Titan's organic haze. *Planet. Space Sci.* 44, 741–747.
- McKay, C.P., Pollack, J.B., Courtin, R., 1989. The thermal structure of Titan's atmosphere. *Icarus* 80, 23–53.
- McKay, C.P., Pollack, J.B., Courtin, R., 1991. The greenhouse and anti-greenhouse effects on Titan. *Science* 253, 1118–1121.
- McKay, C.P., Toon, O.B., 1992. Titan's organic haze. In: Kaldeich, B. (Ed.), *Proceedings, Symposium on Titan*, Vol. ESA SP-338, European Space Agency Publications Division, Noordwijk, pp. 185–190.
- Moses, J.I., Allen, M., Yung, Y.L., 1992. Hydrocarbon nucleation and aerosol formation in Neptune's atmosphere. *Icarus* 99, 318–346.
- Muhleman, D.O., Grossman, A.W., Butler, B.J., Slade, M.A., 1990. Radar reflectivity of Titan. *Science* 248, 975–980.
- Niemann, H. et al., 1997. The gas chromatograph mass spectrometer aboard Huygens. In: Wilson, A. (Ed.), *Huygens: Science, Payload and Mission*, Vol. ESA-SP 1177, European Space Agency Publications Division, Noordwijk, pp. 85–108.
- Podolak, M., Bar-Nun, A., 1979. A constraint on the distribution of Titan's atmospheric aerosol. *Icarus* 39, 272–276.
- Pruppacher, H.R., Klett, J.D., 1978. *Microphysics of Clouds and Precipitation*. D. Reidel, Dordrecht.
- Rages, K.A., Pollack, J.B., 1983. Vertical distribution of scattering hazes in Titan's upper atmosphere. *Icarus* 55, 50–62.
- Rages, K., Pollack, J.B., Smith, P.H., 1983. Size estimates of Titan's aerosols based on Voyager 1 high-phase-angle images. *J. Geophys. Res.* 88, 8721–8728.
- Rannou, P., Cabane, M., Botet, R., Chassefière, E., 1997. A new interpretation of the scattered light at Titan's limb. *J. Geophys. Res.* 102, 10,997–11,013.
- Rannou, P., Cabane, M., Chassefière, E., 1993. Growth of aerosols in Titan's atmosphere and related time scales: a stochastic approach. *Geophys. Res. Lett.* 20, 967–970.
- Rannou, P., Cabane, M., Chassefière, E., Botet, R., McKay, C.P., Courtin, R., 1995. Titan's geometric albedo: role of the fractal structure of the aerosols. *Icarus* 118, 355–372.
- Rannou, P., McKay, C.P., Botet, R., Cabane, M., 1999. Semi-empirical model of absorption and scattering of isotropic fractal aggregates of spheres. *Planet. Space Sci.* 47, 385–396.
- Raulin, F., 1985. Chimie organique dans Titan: expériences de simulation en laboratoire et spéculations. In: Wilson, A. (Ed.), *Huygens*:

- Science, Payload and Mission, ESA-SP 1177, European Space Agency Publications Division, Noordwijk, pp. 161–173.
- Raulin, F., 1987. Organic chemistry in the oceans of Titan. *Adv. Space Res.* 7 (5), 71–81.
- Sagan, C., Dermott, S.F., 1982. The tide in the seas of Titan. *Nature* 300, 731–733.
- Sagan, C., Thompson, W.R., 1984. Production and condensation of organic gases in the atmosphere of Titan. *Icarus* 59, 133–161.
- Sagan, C., Thompson, W.R., Khare, B.N., 1992. Titan: a laboratory for prebiological organic chemistry. *Acc. Chem. Res.* 25, 286–292.
- Samuelson, R.E., 1970. Non-local thermodynamic equilibrium in cloudy planetary atmospheres. *J. Atmos. Sci.* 27, 711–720.
- Samuelson, R.E., 1983. Radiative equilibrium model of Titan's atmosphere. *Icarus* 53, 364–387.
- Samuelson, R.E., Hanel, R.A., Kunde, V.G., Maguire, W.C., 1981. Mean molecular weight and hydrogen abundance of Titan's atmosphere. *Nature* 292, 688–693.
- Samuelson, R.E., Maguire, W.C., Hanel, R.A., Kunde, V.G., Jennings, D.E., Yung, Y.L., Aikin, A.C., 1983. CO₂ on Titan. *J. Geophys. Res.* 88, 8709–8715.
- Samuelson, R.E., Mayo, L.A., 1991. Thermal infrared properties of Titan's stratospheric aerosol. *Icarus* 91, 207–219.
- Samuelson, R.E., Mayo, L.A., 1997. Steady-state model for methane condensation in Titan's troposphere. *Planet. Space Sci.* 45, 949–958.
- Samuelson, R.E., Mayo, L.A., Knuckles, M.A., Khanna, R.J., 1997a. C₄N₂ ice in Titan's north polar stratosphere. *Planet. Space Sci.* 45, 941–948.
- Samuelson, R.E., Nath, N.R., Borysow, A., 1997b. Gaseous abundances and methane supersaturation in Titan's troposphere. *Planet. Space Sci.* 45, 959–980.
- Scattergood, T.W., Lau, E.Y., Stone, B.M., 1992. Titan's aerosols. I. Laboratory investigations of shapes, size distributions, and aggregation of particles produced by UV photolysis of model Titan atmospheres. *Icarus* 99, 98–105.
- Sicardy, B., et al., 1990. Probing Titan's atmosphere by stellar occultation. *Nature* 343, 350–353.
- Smith, B.A., et al., 1981. Encounter with Saturn: Voyager 1 imaging science results. *Science* 212, 163–191.
- Smith, B.A. et al., 1982. A new look at the Saturn system: the Voyager 2 images. *Science* 215, 504–537.
- Smith, P.H., Lemmon, M.T., Lorenz, R.D., Sromovsky, L.A., Caldwell, J.J., Allison, M.D., 1996. Titan's surface, revealed by HST imaging. *Icarus* 119, 336–349.
- Sromovsky, L.A., Suomi, V.E., Pollack, J.B., Kraus, R.J., Limaye, S.S., Owen, T., Revercomb, H.E., Sagan, C., 1981. Implications of Titan's north-south brightness asymmetry. *Nature* 292, 698–702.
- Stevenson, D.J., 1992. The interior of Titan. In: Kaldeich, B. (Ed.), *Symposium on Titan*, Vol. ESA SP-338, European Space Agency Publications Division, Noordwijk, pp. 17–22.
- Tanguy, L., Bézard, B., Marten, A., Gautier, D., Gérard, E., Paubert, G., Lecacheux, A., 1990. Stratospheric profile of HCN on Titan from millimeter observations. *Icarus* 85, 43–57.
- Thompson, W.R., Henry, T.J., Schwartz, J.M., Khare, B.N., Sagan, C., 1991. Plasma discharge in N₂ + CH₄ at low pressures: experimental results and applications to Titan. *Icarus* 90, 57–73.
- Thompson, W.R., McDonald, G.D., Sagan, C., 1994. The Titan haze revisited: magnetospheric energy sources and quantitative tholin yields. *Icarus* 112, 187–199.
- Thompson, W.R., Sagan, C., 1984. Titan: far-infrared and microwave remote sensing of methane clouds and organic haze. *Icarus* 60, 236–259.
- Tokano, T., Neubauer, F.M., Laube, M., McKay, C.P., 1999. Seasonal variation of Titan's atmospheric structure simulated by a general circulation model. *Planet. Space Sci.* 47, 493–520.
- Tomasko, M.G., Smith, P.H., 1982. Photometry and polarimetry of Titan: Pioneer 11 observations and their implications for aerosol properties. *Icarus* 51, 65–95.
- Tomasko, M.G. et al., 1997. The descent imager/spectral radiometer (DISR) aboard Huygens. In: Wilson, A. (Ed.), *Huygens: Science, Payload and Mission*, Vol. ESA-SP 1177, European Space Agency Publications Division, Noordwijk, pp. 109–138.
- Toon, O.B., McKay, C.P., Pollack, J.B., 1980. A physical model of Titan's aerosols. *Icarus* 43, 260–282.
- Toon, O.B., McKay, C.P., Courtin, R., Ackerman, T., 1988. Methane rain on Titan. *Icarus* 75, 255–284.
- Toon, O.B., McKay, C.P., Griffith, C.A., Turco, R.P., 1992. A physical model of Titan's aerosols. *Icarus* 95, 24–53.
- Toublanc, D., Parisot, J.P., Brillet, J., Gautier, D., Raulin, F., McKay, C.P., 1995. Photochemical modeling of Titan's atmosphere. *Icarus* 113, 2–26.
- Trafton, L., 1972. The bulk composition of Titan's atmosphere. *Astrophys. J.* 175, 295–306.
- Veverka, J., 1973. Titan: polarimetric evidence for an optically thick atmosphere. *Icarus* 18, 657–660.
- West, R.A., 1991. Optical properties of aggregate particles whose outer diameter is comparable to the wavelength. *Appl. Opt.* 30, 5316–5324.
- West, R.A., Smith, P.H., 1991. Evidence for aggregate particles in the atmospheres of Titan and Jupiter. *Icarus* 90, 330–333.
- West, R.A., Lane, A.L., Hart, H., Simmons, K.E., Hord, C.W., Coffeen, D.L., Esposito, L.W., Sato, M., Pomphrey, R.B., 1983. Voyager 2 photopolarimeter observations of Titan. *J. Geophys. Res.* 88, 8699–8708.
- Yung, Y.L., 1987. An update of nitrile photochemistry on Titan. *Icarus* 72, 468–472.
- Yung, Y.L., Allen, M., Pinto, J.P., 1984. Photochemistry of the atmosphere of Titan: comparison between model and observations. *Astrophys. J. Suppl.* 55, 465–506.
- Zarnecki, J.C. et al., 1997. The Huygens surface science package. In: Wilson, A. (Ed.), *Huygens: Science, Payload and Mission*, Vol. ESA-SP 1177, European Space Agency Publications Division, Noordwijk, pp. 177–195.
- Zellner, B., 1973. The polarization of Titan. *Icarus* 18, 661–664.